Quercetin activates the SIRT6-Nrf2 axis during oxidative stress, modulating ageing-associated markers

Authors:

Ciara G. Juan[1]*, Nina Simunic-Briski[2], Fabiana Volpe Zanutto[3], Kyle Matchett[4], Gareth W. Davison[1]

Affiliations:

1. Faculty of Life & Health Sciences, Ulster University, York Street, Belfast, BT15 1ED, Northern Ireland, United Kingdom
2. Genos Gylcoscience Research Laboratory Ltd., 10000 Zagreb, Croatia
3. School of Biomedical Sciences, Ulster University, Coleraine, Northern Ireland, BT52 1SA
4. Personalised Medicine Centre, School of Medicine, Ulster University, Derry~Londonderry, Northern Ireland, United Kingdom

*Corresponding author:

Ciara G. Juan

Faculty of Life & Health Sciences, Ulster University, York Street, Belfast, BT15 1ED, Northern Ireland, United Kingdom

Email: juan-ca@ulster.ac.uk

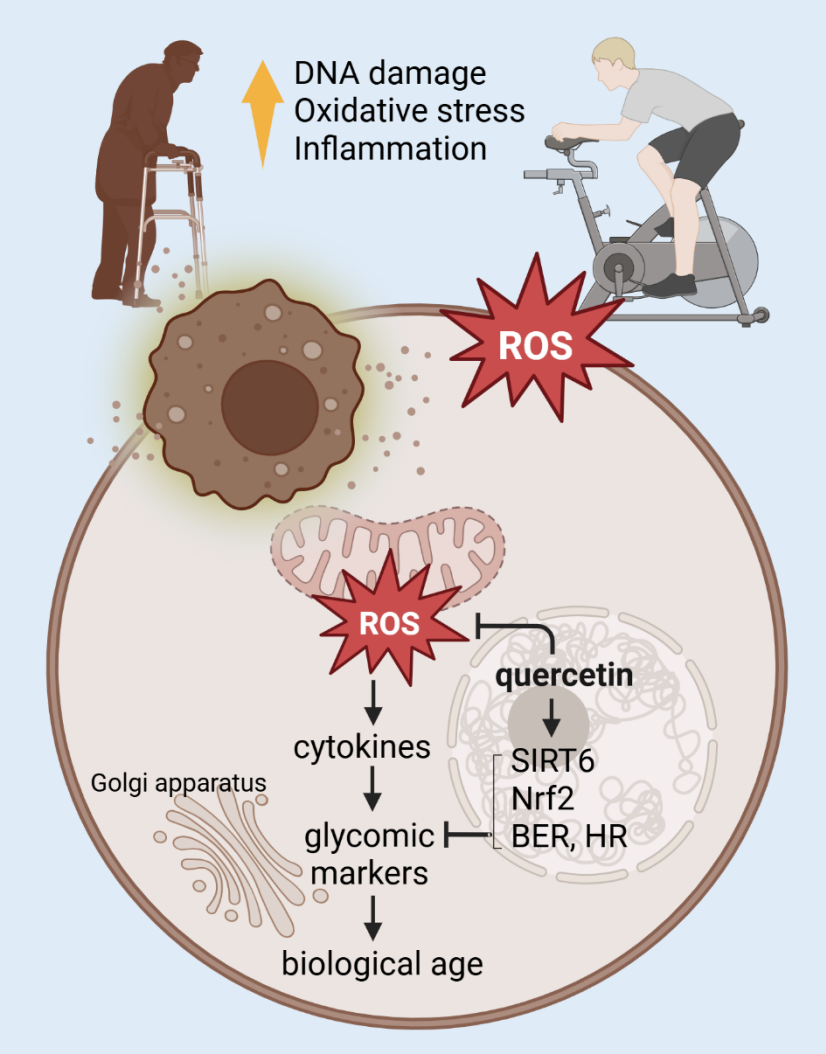

Graphical abstract

Abstract

Quercetin is a dietary flavonoid with antioxidant, anti-inflammatory, and senolytic properties, yet its effects on the DNA damage response and inflammatory markers in healthy humans remain unclear. We conducted a double-blind, placebo-controlled crossover trial in n = 13 apparently healthy male participants, using acute high-intensity interval exercise (HIIE) as the primary stimulus to induce DNA damage and repair combined with acute and 21-day quercetin supplementation (1000 mg/day). Plasma quercetin concentrations and intracellular nuclear localisation was quantified alongside the transcription of several DNA repair genes and sirtuin molecules (*SIRT1*, *SIRT6*), markers of DNA damage (single-strand breaks, oxidised purine bases, double-strand breaks), and IgG and plasma glycomic profiles, including a preliminary GlycanAge index of biological age to characterise molecular and systemic adaptations. Quercetin accumulated in plasma and exhibited enhanced nuclear localisation post-exercise ($p < 0.001$ and $p < 0.05$, respectively). Compared to placebo, quercetin supplementation increased the post-exercise SIRT6-quercetin nuclear colocalisation ($p < 0.001$ in all timepoints) and Nrf2 nuclear translocation ($p < 0.001$). Gene expression of *SIRT1, PARP1,* and *RAD51* increased post-exercise in placebo ($p < 0.05$ in all timepoints), but not in quercetin. Meanwhile, *SIRT6* and *OGG1* expression decreased post-exercise in placebo ($p < 0.05$ in all timepoints), but increased post-exercise in quercetin ($p < 0.05$ in all timepoints). Oxidative DNA damage markers were reduced in the quercetin arm compared to placebo ($p < 0.001$ in all timepoints). Glycomic analysis revealed significant increases in digalactosylation and total galactosylation and a significant decrease in agalactosylation post-exercise (all $p < 0.05$) in placebo, but not in the quercetin arm, suggesting that quercetin attenuated exercise-induced inflammatory glycan shifts. There was a non-significant trend towards increased GlycanAge post-exercise in placebo, and a non-significant decrease post-exercise after short-term quercetin supplementation. In summary, short-term quercetin supplementation activated the SIRT6-Nrf2 axis during exercise-induced oxidative stress, sustaining DNA repair capacity, and modulating systemic inflammatory glycomic markers. These findings provide mechanistic insights into how dietary polyphenols modulate redox-sensitive nuclear and post-translational markers of inflammageing *in vivo*.

Keywords: Quercetin; SIRT6; SIRT1; Nrf2; DNA repair; high-intensity interval exercise; GlycanAge; biological age

Introduction

Oxidative stress arises when the generation of reactive oxygen and nitrogen species (RONS) surpasses the capacity of endogenous antioxidant defences to neutralise them [1]. This imbalance leads to the oxidation of lipids, proteins, and nucleic acids, with DNA being a particularly susceptible target due to its constant exposure to metabolic by-products and environmental insults [2]. Oxidative DNA lesions encompass base modifications such as 8-oxo-7,8-dihydroguanine (8-oxoG), abasic sites, and both single and double-strand breaks, which can compromise genomic integrity if not efficiently repaired [3]. In mammalian cells, several tightly regulated repair pathways maintain DNA stability: the base excision repair (BER) pathway recognises and excises oxidised bases and single-strand breaks through the coordinated activity of DNA glycosylases such as OGG1, XRCC1, and PARP1, while double-strand breaks are resolved through either homologous recombination (HR), mediated by RAD51 and BRCA1/2, or non-homologous end joining (NHEJ), orchestrated by Ku70/Ku80, XRCC4, and DNA-PKcs, with HR providing high-fidelity repair, and NHEJ being faster but more error-prone [4,5]. With advancing age, redox imbalance, chronic inflammation, and reduced NAD^+ bioavailability attenuate the activity of DNA repair enzymes and sirtuins, culminating in the accumulation of persistent DNA damage, genomic instability, and tissue dysfunction [6,7]. Enhancing DNA repair capacity and redox homeostasis is therefore a central focus of emerging geroprotective interventions aimed at promoting healthy ageing.

Acute high-intensity interval exercise (HIIE) is a non-pharmacological, ethically acceptable, physiologically relevant model of oxidative stress and DNA damage [8-10]. Meanwhile, repeated moderate to high-intensity exercise training induce transient oxidative stress that elicits adaptive upregulation of endogenous antioxidant and DNA repair systems [11,12]. This hormetic response involves activation of redox-sensitive transcription factors such as Nrf2, FOXO, and PGC-1α, leading to increased expression of antioxidant enzymes and activity of DNA repair factors [9,11-16]. Both experimental and epidemiological studies report that regular exercise reduces baseline DNA strand breaks,

enhances repair kinetics following oxidative challenge, and mitigates age-related increases in genomic damage [11,17-20]. Mechanistically, reactive oxygen and nitrogen species (RONS) generated during muscle contraction—primarily H_2O_2—serve as critical second messengers that activate the NF-κB and MAPK cascades, two central pathways in redox-regulated gene expression [8]. RONS transiently oxidise cysteine residues on protein tyrosine phosphatases, sustaining kinase phosphorylation and activating the IκB kinase (IKK) complex, which liberates NF-κB to bind promoter regions of antioxidant genes such as *MnSOD* and *GPX*. Concurrently, exercise stimulates phosphorylation of ERK1/2, JNK, and p38MAPK, which phosphorylate downstream transcription factors and reinforce NF-κB-dependent antioxidant gene transcription [8]. This cross-talk between MAPK and NF-κB ensures integrated regulation of antioxidant enzymes, nitric oxide synthase, and mitochondrial biogenesis via PGC-1α, contributing to the long-term enhancement of oxidative stress tolerance [8].

From a nutritional perspective, quercetin, a polyphenolic flavonol, possesses complementary bioactivities that intersect with exercise-induced adaptive pathways. Beyond its well-characterised radical-scavenging capacity, quercetin exerts pleiotropic effects on key regulators of metabolism, DNA repair, and inflammation [21]. It activates AMPK and sirtuin signalling (particularly SIRT1 and SIRT6), enhances Nrf2–Keap1 pathway activation, and modulates NF-κB-mediated inflammatory responses [22-26]. Structural and molecular docking studies have demonstrated direct binding of quercetin to SIRT6 and AMPK catalytic domains, suggesting a potential for allosteric activation of pathways integral to chromatin stability, BER efficiency, and NAD^+ homeostasis [23,27,28]. In animal models, quercetin has been shown to reduce oxidative DNA damage, upregulate OGG1 and XRCC1, and attenuate senescence-associated secretory phenotypes, supporting its classification as a candidate senolytic and DNA repair modulator [29-33].

Despite robust evidence for exercise and quercetin as individual modulators of redox and repair pathways, their combined effects on oxidative DNA damage and repair in humans remain poorly characterised. Understanding whether quercetin can augment or synergise

with exercise-induced DNA damage response is critical for developing integrative lifestyle and nutritional strategies to mitigate age-related genomic instability. The present study was therefore designed to examine the effects of HIIE and quercetin supplementation—individually and in combination—on molecular and biochemical markers of DNA damage and repair in healthy middle-aged men. By coupling quantitative measures of DNA damage and repair with inflammatory biomarkers, this study provides a comprehensive assessment of how exercise and quercetin jointly influence the cellular processes governing oxidative stress resilience and genomic maintenance.

Methods

Participants

Thirteen (n = 13) male participants, between 30-45 years of age (36 ± 4.4 years), of normal weight (BMI 24.5 ± 3.4), light to moderately active (37.6 ± 4.3 $\dot{V}O_2max$) with no medical conditions known to affect responses to exercise and quercetin supplementation took part in this study. Inclusion/exclusion criteria are published elsewhere: https://www.isrctn.com/ISRCTN34136514.

Quercetin Supplementation

In a randomised, double-blind, placebo-controlled, crossover design, all participants received both quercetin and its placebo counterpart in random order. Each short-term supplementation phase lasted 21 days, during which participants ingested 1000 mg of quercetin aglycone dihydrate (DoNotAge.org, UK) or matched placebo capsules once daily with breakfast. Capsules were composed of vegetarian hydroxypropyl methylcellulose (HPMC); the placebo contained rice flour blended with yellow-green food colouring to mimic the appearance of the quercetin capsules. Participants were instructed to refrain from taking additional antioxidant supplements and to maintain their habitual diet and activity patterns throughout the study.

A two to three-week washout period separated the placebo and quercetin treatment phases to ensure complete clearance of quercetin and its metabolites and to minimise

carry-over effects. This duration was based on human pharmacokinetic data showing a terminal elimination half-life of approximately 11 h for quercetin glycosides [34] and on bioequivalence guidance recommending that washout intervals exceed about five elimination half-lives to avoid residual effects [35]. Considering quercetin's enterohepatic recycling and tissue retention, the adopted two to three-week interval corresponds to >30 half-lives, ensuring negligible systemic levels before crossover.

In addition to the short-term supplementation phase, acute supplementation (the first administered dose of quercetin or placebo) was also evaluated. HIEE sessions were conducted at the start (Day 1) and end (Day 21) of each supplementation phase, enabling within-subject comparisons of acute and short-term (21-day) effects of quercetin versus placebo, both before and after exercise-induced oxidative stress. Specifically, the supplement (or its placebo counterpart) was administered 1 hour before exercise, and blood samples were obtained immediately before supplementation and immediately post-exercise. The study design is illustrated in Figure 1.

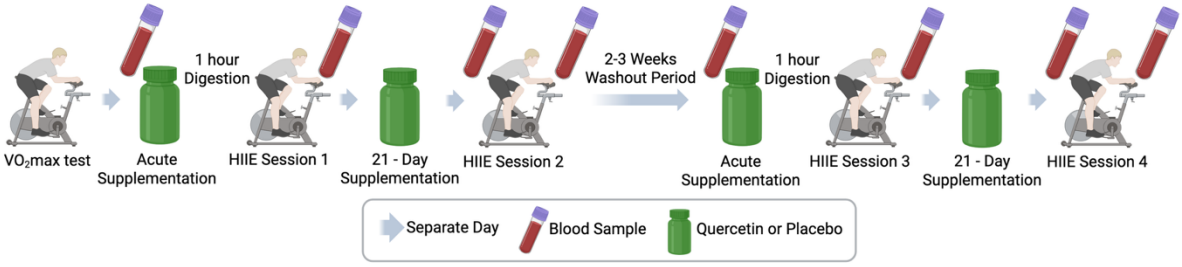

Figure 1. Crossover trial design.

$\dot{V}O_2$max and Experimental Testing

$\dot{V}O_2$max was assessed to prescribe individualised relative exercise intensities for the experimental sessions, ensuring a comparable metabolic load across participants and between time points. Target workloads at 50%, 70%, and 95% of $\dot{V}O_2$max were derived from each participant's incremental test and used to standardise the warm-up, recovery, and work intervals, respectively.

$\dot{V}O_2$max was determined on an electronically braked cycle ergometer (Lode Corival CPET, Lode B.V., Groningen, The Netherlands) using a stepwise ramp protocol in which workload increased by 50 W every 5 min until volitional exhaustion. Breath-by-breath gas exchange was continuously measured (Cosmed Quark CPET, Cosmed, Rome, Italy) following standard two-point gas and flow calibration. $\dot{V}O_2$ values were time-averaged, and the highest 30-s mean was recorded as $\dot{V}O_2$max. Individual $\dot{V}O_2$ work-rate relationships were plotted in Microsoft Excel and fitted by linear regression to estimate the power outputs corresponding to 50%, 70%, and 95% $\dot{V}O_2$max for subsequent exercise sessions.

A standardised 4 × 4 min high-intensity interval exercise (HIIE) protocol was then implemented. Each session began with a 10-min warm-up at approximately 50% $\dot{V}O_2$max, followed by four 4-min work bouts at approximately 95% $\dot{V}O_2$max, interspersed with 3-min active recoveries at approximately 70% $\dot{V}O_2$max. The prescribed powers for the warm-up, recovery, and work intervals were taken from each participant's regression-derived targets to ensure intensity precision and reproducibility across both the acute (day 1) and short-term (day 21) testing phases.

Haematology

Venous blood samples (eight per participant) were collected at the following time points: 1) day 1 of quercetin ingestion at rest; 2) day 1 of quercetin ingestion post-exercise; 3) day 21 of quercetin ingestion at rest; 4) day 21 of quercetin ingestion post- exercise; 5) day 1 of placebo ingestion at rest; 6) day 1 of placebo ingestion post- exercise; 7) day 21 of placebo ingestion at rest; and 8) day 21 of placebo ingestion post- exercise.

Blood was drawn from the antecubital fossa of the non-dominant arm using a 21-gauge butterfly needle while participants were in a supine position to minimise venous pooling and physiological variability. Samples were collected into a combination of EDTA, serum-separator, and PAXgene RNA vacutainers (BD Biosciences, Franklin Lakes, NJ, USA; PreAnalytiX, Hombrechtikon, Switzerland) to allow downstream molecular and biochemical analyses.

EDTA and serum-separator tubes were centrifuged within 30 min of collection at 1500 × g for 10 min at 4 °C. Plasma and serum were aliquoted (1 mL) into sterile cryovials and stored at −80 °C until analysis of oxidative stress and glycomic markers.

Whole blood collected in PAXgene tubes was gently inverted 10 times immediately after collection, kept at room temperature for 2 h to ensure complete lysis, then stored at −20 °C overnight before transfer to −80 °C for long-term storage pending RNA extraction.
All samples were labelled with anonymised participant IDs, treatment phase, and time point, and were maintained on ice throughout handling. Freeze-thaw cycles were avoided to preserve molecular integrity.

In addition to venous sampling, arterialised capillary blood was obtained by finger-prick for the determination of haemoglobin and haematocrit using the equations described by Dill and Costill [36] (Supplementary Table S1). All collections were performed between 09:00 and 10:00 to minimise diurnal variation in molecular responses to exercise [37]. Immediately following baseline blood sampling, participants commenced the HIIE session. Post-exercise blood draws were collected immediately after cooldown.

Plasma Quercetin and Cell Uptake

Blood quercetin aglycone concentrations were determined using ultra-high-performance liquid chromatography coupled with tandem mass spectrometry (UHPLC–MS/MS), as previously described for plasma flavonol quantification in human supplementation studies [38]. A total of 100 µL plasma was mixed with 300 µL acetonitrile (≥99.9 %, LC–MS grade; Sigma-Aldrich, St Louis, MO, USA) to precipitate proteins, vortex-mixed for 30 s, and centrifuged for 15 min at 1500 × g, 4 °C. The supernatant was extracted with 300 µL ethyl acetate (≥99.8 %, Sigma-Aldrich), vortex-mixed for 30 s, and centrifuged again under identical conditions. 250 µL of the resulting supernatant was transferred to a 5 mL borosilicate glass vial (Agilent Technologies, Waldbronn, Germany) and evaporated to dryness under a gentle stream of nitrogen using a Techne Dri-Block DB-3D sample concentrator (Techne, Staffordshire, UK) at room temperature for 30 min. The residue

was reconstituted in 100 µL acetonitrile, sonicated for 10 s, vortex-mixed for 30 s, and transferred to UHPLC vials for analysis. All samples and standards were processed in parallel under subdued light to minimise quercetin degradation.

Analyses were performed on an Agilent 1200 Series UHPLC system (Agilent Technologies, Waldbronn, Germany) equipped with an autosampler and thermostat column compartment, coupled to a Sciex Triple Quad 5500+ mass spectrometer (AB Sciex LLC, Framingham, MA, USA) with an electrospray ionisation (ESI) source operating in negative ion mode. Separation was achieved on a ZORBAX Eclipse XDB-C18 column (4.6 × 150 mm, 5 µm; Agilent Technologies) maintained at 30 °C. The mobile phases consisted of (A) water with 0.1 % (v/v) formic acid (Honeywell, Charlotte, NC, USA) and (B) acetonitrile (LC–MS grade; Sigma-Aldrich). A linear gradient was applied as follows: 0–2 min, 30 % B; 2–10 min, 30–80 % B; 10–12 min, 80 % B; 12–14 min, return to 30 % B for re-equilibration. The flow rate was 1.0 mL min^{-1} and the injection volume 10 µL.

Typical MS source parameters were: ion-spray voltage −4500 V, nebuliser gas (GS1) 50 psi, auxiliary gas (GS2) 60 psi, curtain gas 30 psi, and source temperature 350 °C. Multiple reaction monitoring (MRM) transitions were monitored for quercetin aglycone (precursor m/z 301.0 → product m/z 151.0 and 179.0; dwell time 50 ms per transition). Collision energy and declustering potentials were optimised using authentic quercetin aglycone standards (≥98 %, Sigma-Aldrich). Calibration standards were prepared by spiking blank human plasma with known concentrations of quercetin aglycone (1–200 ng mL^{-1}) and processed identically to study samples. Peak areas were integrated using Analyst 1.8.2 software (AB Sciex), and calibration curves were generated by weighted (1/x) linear regression in Microsoft Excel. Concentrations of unknown samples were interpolated from the standard curve.

To assess intracellular uptake of native quercetin and its colocalisation with SIRT6, PBMCs collected before and after quercetin and placebo supplementation were analysed using super-resolution microscopy, following established protocols for quercetin

autofluorescence and SIRT6 immunofluorescence [39,40]. Cells were stored at −80 °C in cryopreservation medium containing 10 % dimethyl sulfoxide (DMSO; Sigma-Aldrich, St Louis, MO, USA) and fetal bovine serum (FBS; Gibco, Thermo Fisher Scientific, Waltham, MA, USA). For analysis, cells were thawed in a 37 °C water bath, diluted in pre-warmed RPMI-1640 medium (Gibco) containing 10 % FBS, and centrifuged to remove DMSO. A total of 200 µL lymphocytes was spotted onto Superfrost Plus slides (Thermo Fisher Scientific) and allowed to adhere for 15 min. Cells were fixed with 4 % paraformaldehyde in PBS (Sigma-Aldrich) for 10 min, washed three times in PBS (Sigma-Aldrich), and permeabilised with 0.5 % Triton X-100/PBS (Sigma-Aldrich) for 10 min. Non-specific binding was blocked with 2.5 % normal horse serum (NHS; Vector Laboratories, Burlingame, CA, USA) for 1 h. Slides were then incubated with rabbit polyclonal anti-SIRT6 antibody (1:500; Proteintech, 28677-1-AP, Manchester, UK) in 1 % NHS/PBS for 1 h at room temperature, washed three times in 0.05 % Tween-20/1 % NHS/PBS, and incubated with goat anti-rabbit Alexa Fluor 568 antibody (1:500; Invitrogen, Thermo Fisher Scientific) for 1 h.

Quercetin autofluorescence was visualised directly in the green channel (excitation 488 nm), eliminating the need for secondary staining. Nuclei were counterstained with Vectashield Antifade Mounting Medium containing DAPI (Vector Laboratories) and coverslipped with clear nail polish. High-resolution images were acquired using a Leica Stellaris One Tau 3D STED Nanoscope (Leica Microsystems, Wetzlar, Germany) with a 100×/1.4 NA oil-immersion objective. Excitation/emission settings were: DAPI (Ex 405 nm, Em 415–480 nm; gain 5 %, laser 10 %), Alexa Fluor 488 (Ex 488 nm, Em 500–550 nm; gain 30 %, laser 100 %), and Alexa Fluor 568 (Ex 561 nm, Em 570–620 nm; gain 30 %, laser 70 %). Sequential scanning was used to prevent spectral cross-talk. For each field of view, Z-stacks were captured spanning the full nuclear depth, with all imaging parameters (laser power, detector gain, and pinhole size) held constant. Each image contained ≥ 40 nuclei, and at least three independent fields (≥ 100 nuclei total) were analysed per condition.

Three-dimensional image stacks were processed using Imaris 10.2 (Oxford Instruments, UK). Raw STED data were converted to Imaris format and subjected to automated colocalisation analysis. Thresholds for quercetin (green; Alexa Fluor 488) and SIRT6 (red; Alexa Fluor 568) channels were set to 90, and for DAPI to 20, based on the faintest visible foci within each batch. Nuclear volumes were segmented from the DAPI channel using the Surface module, and spot detection was applied separately to quercetin and SIRT6 channels. Colocalisation was quantified using the Colocalisation module, reporting the percentage region of interest (%ROI)—the proportion of the nuclear volume containing overlapping quercetin and SIRT6 signals—as the primary outcome measure. This voxel-based 3D quantification approach was adapted from established Imaris colocalisation workflows [41]. Median fluorescence intensities for green and red channels were quantified for each nucleus using automated batch-processing tools in Imaris. All imaging and analysis parameters (laser power, detector gain, thresholds, segmentation) were held constant across experimental conditions to ensure comparability. Secondary-only and no-primary antibody controls confirmed antibody specificity.

DNA Damage

Three individual markers of DNA damage were assessed: 1) Single-strand breaks using alkaline comet assay; 2) Oxidised purine bases using a modified comet assay with Formamidopyrimidine-DNA Glycosylase (FPG) incubation; and 3) Double-strand breaks (γH2AX and 53BP1 foci colocalisation) using super-resolution 3D microscopy.

Comet assay. The alkaline and FPG-modified comet assays were performed as described by Collins et al. [42]. Cryopreserved PBMCs were thawed at 37 °C, mixed with 9 mL phosphate-buffered saline (PBS; Thermo Fisher Scientific, Waltham, MA, USA), and centrifuged for 7 min at 700 × g, 4 °C. The supernatant was discarded, and the cell pellets were resuspended in 1 mL PBS for seeding. A total of 25 µL resuspended cells was mixed with 150 µL low-melting-point agarose (LMPA; Sigma-Aldrich, St Louis, MO, USA) pre-warmed to 37 °C. Seventy µL of the cell–agarose suspension was layered onto Superfrost Plus microscope slides (Fisherbrand, Thermo Fisher Scientific) pre-coated with 1 %

normal-melting-point agarose (NMPA; Sigma-Aldrich), covered with a 20 × 20 mm coverslip, and allowed to solidify for 5 min at room temperature. After coverslip removal, slides were immersed for 1 h in lysis buffer (2.5 M NaCl, 100 mM Na_2EDTA, 10 mM Tris, 1 % Triton X-100; all from Sigma-Aldrich; pH 10–10.5). Slides were then placed for 20 min in electrophoresis buffer (300 mM NaOH, 1 mM Na_2EDTA; pH 12.5–13) to allow DNA unwinding, followed by electrophoresis at 25 V (≈ 0.15 V cm^{-1}), 300 mA, 4 °C for 30 min. After electrophoresis, slides were neutralised in PBS for 10 min and rinsed with distilled water for 10 min, then air-dried overnight at room temperature.

Slides were stained with SYBR™ Gold nucleic acid stain (Thermo Fisher Scientific) prepared as a 1:1000 dilution in DMSO (Sigma-Aldrich) and mixed with TE buffer (10 mM Tris-HCl, 1 mM EDTA; pH 7.5–8). Slides were immersed in staining solution for 30 min on an orbital shaker at room temperature, washed briefly in distilled water, and mounted with 10 µL distilled water under a coverslip for fluorescence microscopy. Image acquisition was performed using an Olympus BX41 fluorescence microscope (Olympus Corporation, Tokyo, Japan) equipped with a 40× oil-immersion objective. Comet parameters were quantified using Comet Assay IV software (v4.3; Instem Scientific Ltd., Staffordshire, UK), which automatically calculates % DNA in tail. One hundred cells were scored per slide, and the median tail intensity was used as the primary marker of DNA damage, as recommended by Collins et al.[42].

For the modified comet assay with formamidopyrimidine-DNA glycosylase (FPG) incubation, the same steps in the alkaline comet assay were performed, with the addition of FPG incubation. After normal lysis, cells were washed with enzyme buffer (40 mM HEPES, 0.1 M KCl, 0.5 mM EDTA, 0.2 mg/ml BSA) with a pH of 8 for three times. After washing, slides were placed on ice and treated with 7 µL FPG mixed with 50 µL enzyme buffer. To avoid drying, slides were transferred to a glass container lined with wet tissue and covered with aluminum foil and placed in the incubator for 30 minutes at 37 °C. A buffer-only control slide without FPG was included in the incubation step. After incubation, the same alkaline buffer soaking, electrophoresis, staining, and scoring

procedures in the alkaline comet assay were performed. To determine the final damage score, the median tail intensity of the buffer-only control sample was subtracted from the median of the FPG-incubated sample.

Super-resolution 3D microscopy for DNA double-strand break and Nrf2 localisation. DNA double-strand breaks (DSBs) were visualised through γH2AX and 53BP1 co-localisation, while Nrf2 nuclear localisation was assessed by immunofluorescence. Super-resolution 3D confocal and STED imaging provides superior sensitivity for detecting γH2AX/53BP1 foci compared with 2D microscopy, as 2D projections can underestimate DSB foci by ~40 % [43] and confocal microscopy with 3D reconstruction identifies approximately threefold more foci [44]. A total of 200 µL lymphocytes was spotted onto Superfrost Plus slides (Fisherbrand, Thermo Fisher Scientific, USA) and allowed to adhere for 15 min. Cells were fixed with 4% paraformaldehyde in PBS (Sigma-Aldrich, USA) for 10 min, washed three times in PBS, and permeabilised with 0.5 % Triton X-100/PBS (Sigma-Aldrich) for 10 min. Slides were blocked with 2.5 % normal horse serum (NHS; Vector Laboratories, USA) for 1 h, then incubated for 1h with either: anti-phospho-histone H2AX (Ser139, mouse mAb, 1:500; Invitrogen, Thermo Fisher Scientific) together with anti-53BP1 (rabbit pAb, 1:500; Invitrogen, Thermo Fisher Scientific) for DSB analysis, or CoraLite® 594-conjugated anti-Nrf2 (rabbit pAb, 1:500; Proteintech 16396-1-AP, Manchester, UK) for Nrf2 localisation, following established protocols for oxidative-stress–induced Nrf2 activation []. Slides were washed three times in 0.05 % Tween-20/1 % NHS/PBS (Sigma-Aldrich).

For DSB imaging, cells were further incubated with goat anti-mouse Alexa Fluor® 488 IgG (1:500; Invitrogen A-11001) and goat anti-rabbit Alexa Fluor® 568 IgG (1:500; Invitrogen A-11011) for 1 h. Slides were mounted with Vectashield Antifade with DAPI (Vector Laboratories) and sealed with clear nail varnish. Images were acquired using a Leica Stellaris One Tau 3D STED Nanoscope (Leica Microsystems, Germany) with a 100×/1.4 NA oil-immersion objective. Sequential scanning was used to prevent spectral overlap using the following settings for DSB analysis: DAPI (excitation 405 nm; emission 415–480 nm; detector gain 5%, laser power 10%), Alexa Fluor 488 (excitation 488 nm; emission 500–

550 nm; detector gain 30%, laser power 70%), and Alexa Fluor 568 (excitation 561 nm; emission 570–620 nm; detector gain 30%, laser power 70%). For Nrf2: DAPI (excitation 405 nm; emission 415–480 nm; detector gain 5%, laser power 10%) and Alexa Fluor 594 (excitation 593 nm; emission 610–620 nm; detector gain 30%, laser power 70%). Laser power, detector gain, and pinhole size were kept constant. Each field contained ≥ 40 nuclei, with ≥ 3 fields per sample (≥ 100 nuclei total).

Z-stacks were processed in Imaris 10.2 (Oxford Instruments, UK). For DSB analysis, thresholds were set to 1000 (green/red) and 50 (DAPI). Nuclear volumes were segmented from DAPI, and colocalisation was quantified as the percentage region of interest (%ROI)—the proportion of nuclear volume containing overlapping γH2AX and 53BP1 signals—using voxel-based correlation [41]. For Nrf2, median Alexa 594 intensity per nucleus was determined by automated batch analysis. All imaging and analysis parameters were held constant across conditions. Secondary-only and no-primary antibody controls confirmed antibody specificity.

DNA Repair

Whole blood was collected in PAXgene® Blood RNA Tubes (PreAnalytiX GmbH, Hombrechtikon, Switzerland; distributed by Qiagen, Hilden, Germany) to stabilise intracellular RNA immediately after phlebotomy. Total RNA was isolated using the PAXgene® Blood RNA Kit (Qiagen, Hilden, Germany) according to the manufacturer's instructions, including on-column DNase digestion to remove residual genomic DNA. RNA concentration and purity were assessed spectrophotometrically using a NanoDrop™ ND-1000 Spectrophotometer (Thermo Fisher Scientific, Waltham, MA, USA) by measuring A260/A280 ratios.

RNA samples were diluted with nuclease-free water (Ambion, Thermo Fisher Scientific) to ensure exactly 500 ng of total RNA (or up to 1 µg where indicated) per reverse-transcription reaction. Complementary DNA (cDNA) was synthesised using the High-Capacity cDNA Reverse Transcription Kit (Applied Biosystems, Foster City, CA, USA) in a

20 µL reaction (25 °C for 10 min, 37 °C for 120 min, 85 °C for 5 min) following the manufacturer's protocol. Synthesised cDNA was stored at –20 °C until further use.

Each 20 µL qPCR reaction contained 10 µL TaqMan® Universal PCR Master Mix (2×) (Applied Biosystems), 1 µL cDNA template (≈ 25 ng reverse-transcribed RNA), 0.5 µL forward primer (10 µM; final ≈ 250 nM), 0.5 µL reverse primer (10 µM; ≈ 250 nM), 0.5 µL dual-labelled hydrolysis probe (5 µM), and 7.5 µL nuclease-free water (Ambion, Thermo Fisher Scientific). Amplifications were carried out in 96-well optical plates on an Applied Biosystems 7500 Fast Real-Time PCR System using standard cycling conditions: 95 °C for 10 min, followed by 40 cycles of 95 °C for 15 s and 60 °C for 1 min.

All reactions were performed in technical duplicates, and no-template controls were included to verify the absence of contamination. Gene expression was assessed for six DNA repair-related targets (*SIRT1, SIRT6, XRCC1, PARP1, OGG1, RAD51*) using TaqMan® Gene Expression Assays (Applied Biosystems), with half of the probes labelled with VIC® dye and half with FAM™ dye for multiplex detection. Expression data were normalised to the geometric mean of three housekeeping genes (*HPRT1, TUBB, GAPDH*) to account for differences in RNA input and amplification efficiency.Primers and probes (5'→3'):

Gene	**Forward primer**	**Reverse primer**
SIRT1	TAGACACGCTGGAACAGGTTGC	CTCCTCGTACAGCTTCACAGTC
SIRT6	TGGCAGTCTTCCAGTGTGGTGT	CGCTCTCAAAGGTGGTGTCGAA
XRCC1	CGGATGAGAACACGGACAGTGA	GAAGGCTGTGACGTATCGGATG
PARP1	CCAAGCCAGTTCAGGACCTCAT	GGATCTGCCTTTTGCTCAGCTTC
OGG1	GGCTCAACTGTATCACCACTGG	GGCGATGTTGTTGTTGGAGGAAC
RAD51	TCTCTGGCAGTGATGTCCTGGA	TAAAGGGCGGTGGCACTGTCTA
HPRT1	CATTATGCTGAGGATTTGGAAAGG	CTTGAGCACACAGAGGGCTACA
TUBB	CTGGACCGCATCTCTGTGTACT	GCCAAAAGGACCTGAGCGAACA
GAPDH	GTCTCCTCTGACTTCAACAGCG	ACCACCCTGTTGCTGTAGCCAA

Relative gene expression levels were quantified using the ΔCt method, with target gene expression normalised to the geometric mean of three reference genes (HPRT, TUBB, and GAPDH). ΔCt values were exported to IBM SPSS Statistics (Version 31; IBM Corp., Armonk,

NY, USA) for statistical analyses. Fold changes in gene expression were calculated using the $2^{(-\Delta\Delta Ct)}$ method and visualised as bar graphs.

IgG and plasma N-glycan profiling

IgG N-glycans were analysed using a capillary gel electrophoresis with laser-induced fluorescence (CGE-LIF) developed by Hanić et al. [45]. The analysis was performed by isolating IgG from plasma samples, using a Protein G monolithic plate in detail described in the protocol [45], followed by the release and fluorescent labelling of N-glycans. N-glycans were incubated with PNGase F and released from denatured glycoproteins, labelled with 8-aminopyrene-1,3,6-trisulfonic acid trisodium salt (APTS) and purified from salt and excess label by HILIC-based solid phase extraction (HILIC-SPE) [45,46]. CGE-LIF glycoprofiling was performed using a 3130 Genetic Analyser (Applied Biosystems, Waltham, MA, USA). The obtained electropherograms were integrated into 27 peaks using Waters Empower 3 software (Waters, US). The list of the corresponding structures for these peaks is provided in the Supplementary Table S2)

Plasma glycans were isolated from individual plasma samples, denatured by incubation with SDS (Invitrogen, Waltham, MA, USA) at 65 °C for 10 min, followed by the release of glycans with the addition of 1.2 units of peptide: N-glycosidase F (Promega, Madison, MI, USA) and overnight incubation at 37 °C. N-glycans were labelled with 2-aminobenzamide (Sigma-Aldrich, Saint Louis, MO, USA), separated by hydrophilic interaction liquid chromatography on an Acquity Ultra-Performance Liquid Chromatography (UPLC Technology) instrument (Waters, Milford, MA, US), and quantified with a fluorescence detector using the hydrophilic interaction ultra-high-performance liquid chromatography with fluorescence detection (HILIC-UHPLC-FLR) method [45,46]. Chromatograms were separated into 39 glycan peaks (GPs) (the list of all glycan structures is provided in Supplementary Table S2).

GlycanAge

GlycanAge is an index of biological age that estimates how old the body is functionally by analysing the N-glycans attached to IgG—the main antibody circulating in plasma [47,48]. These IgG glycans modulate antibody effector functions and systemic inflammation, and their composition changes predictably with age [48]. GlycanAge measures inflammageing, the chronic, low-grade inflammation that develops progressively with age, even in the absence of infection, and represents a central integrative hallmark that drives or amplifies many other hallmarks of ageing [49]. GlycanAge was derived from IgG glycan peaks quantified using the protocol described above [45]. A trained multivariate regression model (the proprietary GlycanAge algorithm) then predicts biological age from the weighted sum of these traits, typically explaining >60 % of chronological age variance [50,51].

Statistical Analysis

A prospective power calculation was conducted based on prior experimental data examining DNA damage (comet assay) following acute and short-term antioxidant supplementation using a crossover design [52]. The analysis indicated that a minimum of ten participants was required to detect a significant between-group difference ($p < 0.05$) with 85 % power. Data normality was assessed using the Shapiro-Wilk test, and non-normal data were transformed to natural log values prior to analysis. When log-transformed data remained non-normally distributed, non-parametric tests were used. Primary analyses employed a general linear model (GLM) with repeated measures, including Time (pre vs post-exercise) as the within-subject factor and Group (quercetin vs placebo) as the between-subjects factor, to test the Time × Group interaction. For significant interaction effects ($p < 0.05$), post-hoc one-way ANOVA with Tukey correction (or Kruskal-Wallis test for non-parametric data) was applied to compare between-group differences at individual timepoints. Within-subject pre vs post-exercise comparisons were performed using paired t-tests (or Wilcoxon signed-ranks tests for non-parametric data).

To control the family-wise error rate (FWER), a Bonferroni correction with $m = 2$ was applied within each treatment arm, corresponding to the two pre-post exercise contrasts (Day 1 and Day 21). This approach follows international statistical guidance allowing FWER control within pre-specified families of hypotheses that address distinct scientific questions [53,54]. The two to three-week wash-out period, based on pharmacokinetic evidence that quercetin's half-life is ≈ 11 h and regulatory guidance recommending ≥ 5 half-lives for complete elimination, was sufficient to eliminate carryover effects. Consequently, each supplementation phase (quercetin and placebo) was treated as a separate, pre-specified analytical family for multiplicity control, while all inferential tests remained within-subject to account for intra-individual correlation. Results are reported as mean ± SD for normally distributed data and median (IQR) for non-normal data, with significance accepted at $p < 0.05$ (Bonferroni-adjusted where applicable).

Ethical Approval

The human trial was approved by Ulster University Research Ethics Committee (REC/23/0020) and registered in a publicly accessible database recognised by the World Health Organization (ISRCTN34136514).

Results

Retention and Compliance

Participant retention was 54%, yielding a final analytical sample of n = 13. Despite attrition, the general linear model with a repeated-measures design indicated an observed power of 1.00 for the Time × Group interaction, confirming adequate statistical power for the primary outcomes. Supplementation compliance was 100%, as reflected by linear increases in plasma quercetin aglycone levels in every participant, measured by UHPLC–MS/MS.

Quercetin Levels and Uptake

Plasma quercetin aglycone levels increased in all active treatment timepoints ($p < 0.05$). Acute supplementation resulted in significantly higher plasma quercetin levels post-exercise compared to placebo ($p < 0.001$, Figure 2A). Meanwhile, 21-day supplementation resulted in significantly higher quercetin levels both at rest and post-exercise ($p < 0.001$ for both). In addition, nuclear quercetin increased post-exercise in both treatment conditions (all $p < 0.05$). Short-term (21-day) supplementation increased the post-exercise nuclear uptake of quercetin relative to placebo ($p < 0.05$, Figure 2B).

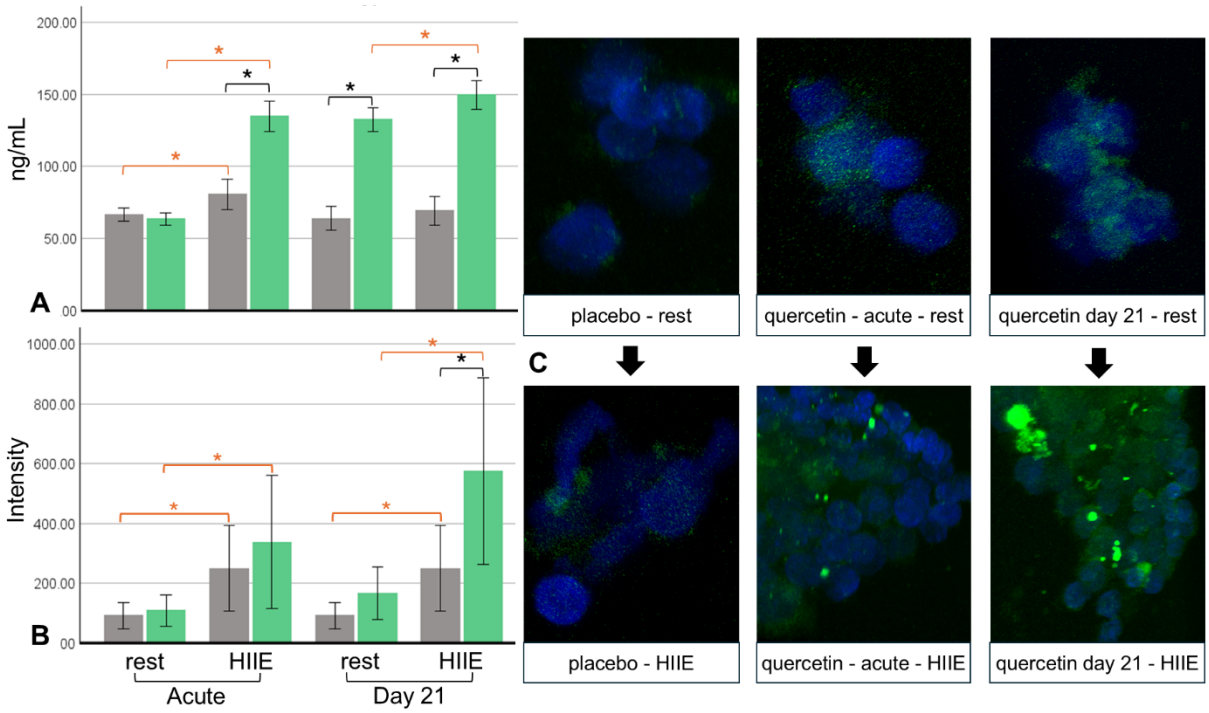

Figure 2. A) Plasma quercetin aglycone levels (ng/ml) following acute and short-term (day 21) phases of supplementation for placebo (grey bars) vs quercetin (green bars); B) Median fluorescence intensity of native, unstained quercetin in nucleus; C) Confocal microscopy of native, unstained quercetin. Black asterisk indicates significant between-group difference. Orange asterisk indicates significant within-subject difference.

DNA Damage

DNA single-strand breaks (comet assay) increased post-exercise in all exercise sessions and conditions ($p < 0.001$ for all timepoints, Figure 3A). Short-term (21-day) supplementation significantly decreased the post-exercise strand break relative to placebo ($p < 0.001$). Similarly, purine base oxidation increased post-exercise in all exercise sessions and conditions ($p < 0.001$ for all timepoints, Figure 3B), with significantly lower oxidation post-exercise in quercetin compared to placebo after short-term supplementation ($p < 0.001$) .

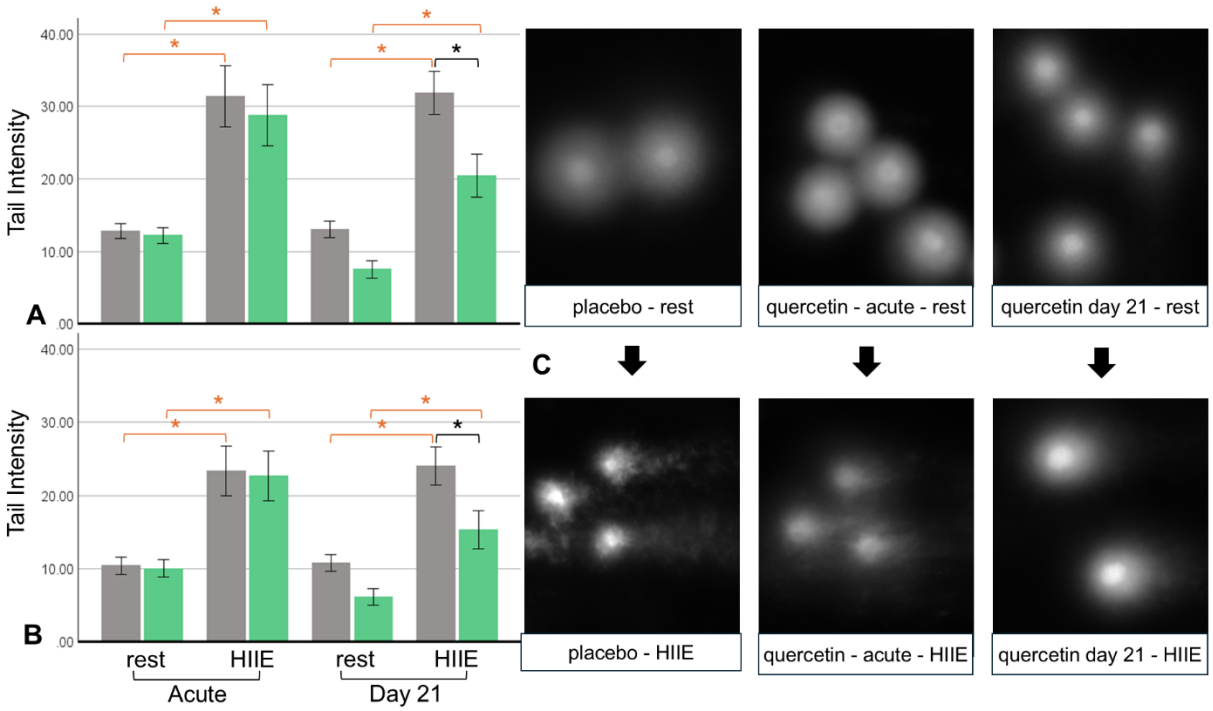

Figure 3. A) DNA strand breaks (tail intensity) quantified by single-cell gel electrophoresis comparing placebo (grey bars) vs quercetin (green bars); B) Oxidised purine bases (tail intensity) with FPG incubation; C) Fluorescence microscopy of DNA fragment migration. Black asterisk indicates significant between-group difference. Orange asterisk indicates significant within-subject difference.

DNA double-strand breaks (colocalisation of yH2AX and 53BP1) increased post-exercise in all exercise sessions and conditions ($p < 0.001$ for all timepoints, Figure 4A). Both acute and short-term quercetin supplementation resulted in lower strand breaks post-exercise compared to placebo ($p < 0.001$ for both).

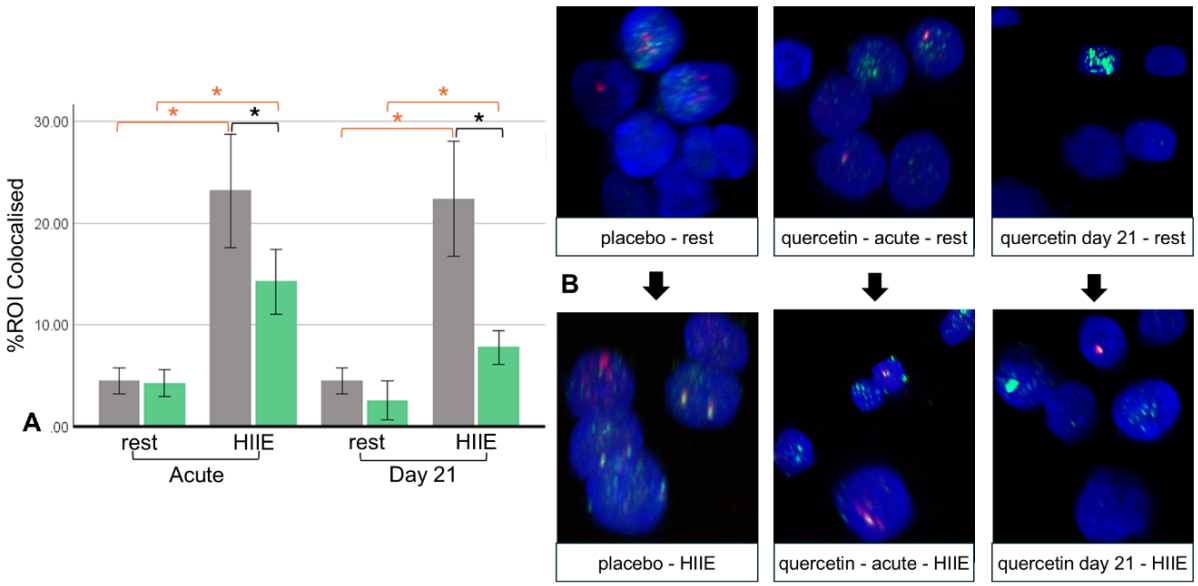

Figure 4. A) DNA double-strand breaks quantified by yH2AX and 53BP1 colocalisation (%ROI colocalised) comparing placebo (grey bars) vs quercetin (green bars); B) confocal microscopy of yH2AX and 53BP1 colocalisation showing white puncta from overlapping green (yH2AX) and red (53BP1). Black asterisk indicates significant between-group difference. Orange asterisk indicates significant within-subject difference.

Transcriptional DNA Repair

SIRT1 expression significantly increased post-exercise in all placebo sessions ($p < 0.05$ for all, Figure 5A), but this effect was attenuated in quercetin. Meanwhile, *SIRT6* significantly decreased in all placebo sessions ($p < 0.05$ for all, Figure 5B), but increased post-exercise after short-term quercetin supplementation ($p < 0.05$). Similar to *SIRT1*, *PARP1* significantly increased post-exercise in all placebo sessions ($p < 0.05$ for all, Figure 5C), with no significant effects in quercetin. Meanwhile, *OGG1*, like *SIRT6*, significantly decreased post-exercise in all placebo sessions ($p < 0.05$ for all, Figure 5D), but significantly increased post-exercise in all quercetin sessions ($p < 0.05$ for all). Finally, *RAD51,* like *SIRT1* and *PARP1,* significantly increased post-exercise in all placebo sessions

(p < 0.05 for all, Figure 5E), with no significant effects in quercetin. There were no significant changes in *XRCC1* expression.

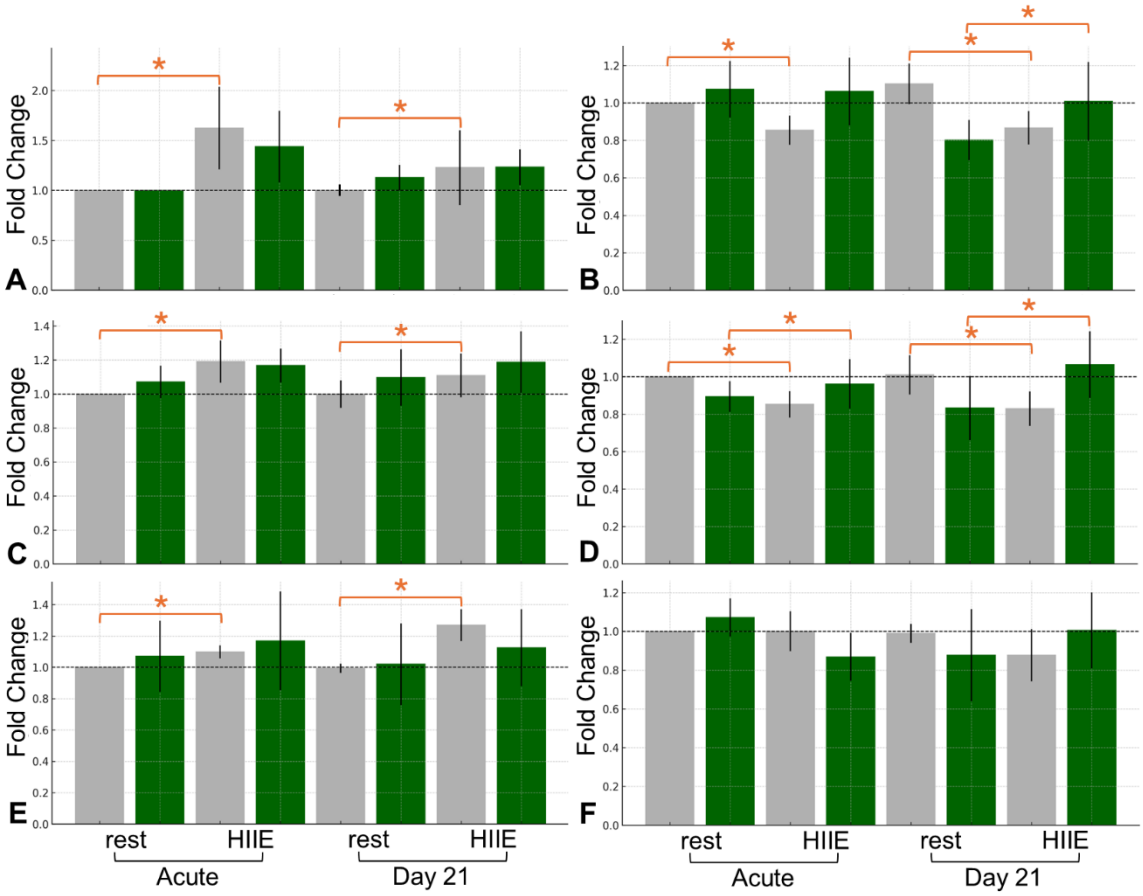

Figure 5. Fold change in A) SIRT1; B) SIRT6; C) PARP1; D) OGG1; E) RAD51; F) XRCC1 comparing placebo (grey bars) vs quercetin (green bars). Orange asterisk indicates significant within-subject difference.

Since SIRT6 has been shown to bind with quercetin, colocalisation of SIRT6 protein with quercetin was quantified using super-resolution 3D microscopy. Post-exercise colocalisation increased in all exercise sessions and conditions (p < 0.001 for all timepoints, Figure 6A). Both acute and short-term supplementation increased the post-exercise colocalisation relative to placebo (p < 0.001 for both). Short-term supplementation also increased resting colocalisation relative to placebo (p < 0.001).

Since SIRT6 mono-ADP-ribosylation activity is essential for transcriptional activation of a subset of Nrf2 target genes under oxidative stress [55], Nrf2 was also imaged. Nuclear Nrf2 increased post-exercise in all exercise sessions and conditions ($p < 0.001$ for all timepoints, Figure 6A). Both acute and short-term quercetin supplementation increased nuclear Nrf2 post-exercise relative to placebo ($p < 0.05$ for both).

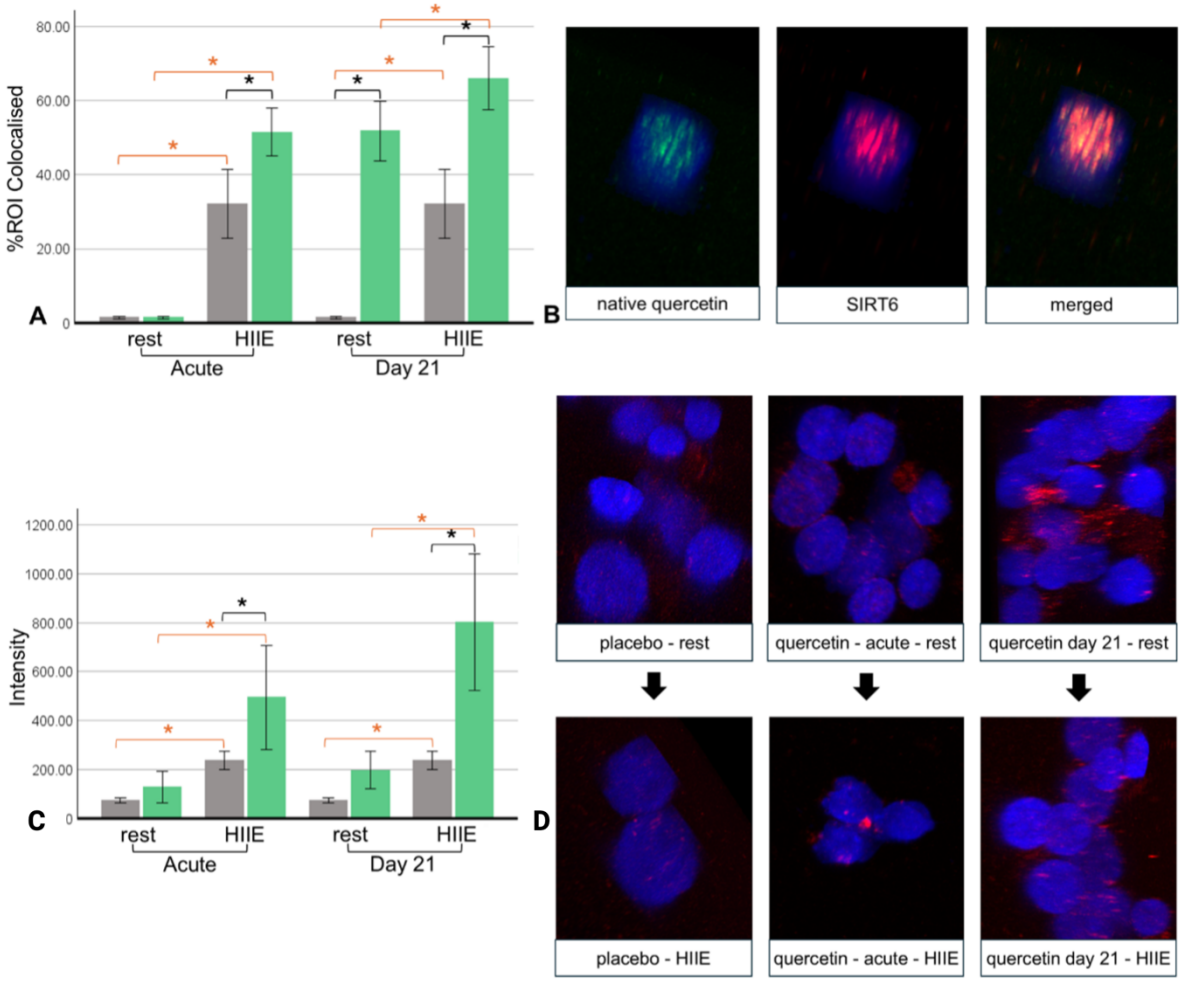

Figure 6. A) SIRT6 colocalisation with native, unstained quercetin (%ROI colocalised) comparing placebo (grey bars) vs quercetin (green bars); B) Confocal microscopy of colocalisation. Black asterisk indicates significant between-group difference. Orange asterisk indicates significant within-subject difference. C) Nuclear Nrf2 (median intensity) comparing placebo (grey bars) vs quercetin (green bars); D) Confocal microscopy of Nrf2 nuclear translocation. Black asterisk indicates significant between-group difference. Orange asterisk indicates significant within-subject difference.

Glycomic Profiling of IgG and Plasma Proteins

Plasma agalactosylation (G0), a pro-inflammatory marker, significantly decreased post-exercise in placebo ($p < 0.05$, Figure 7A), reflecting a reduction in pro-inflammatory agalactosylated structures and suggesting an acute anti-inflammatory response or post-exercise resolution phase. This acute response was not observed in the quercetin arm, suggesting that quercetin supplementation modulated the exercise-induced glycan shift.

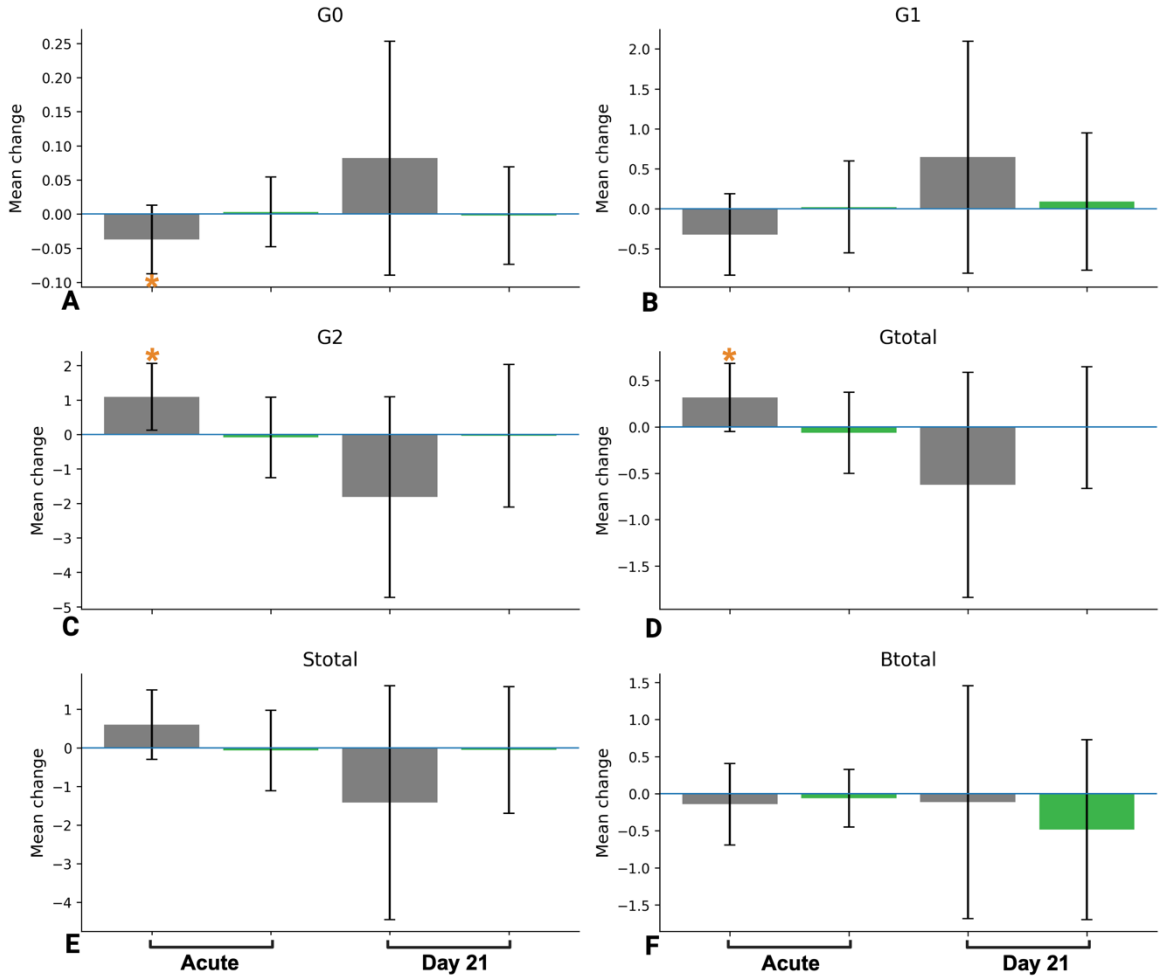

Figure 7. Plasma glycan changes from pre to post-exercise during acute and short-term supplementation. Changes in plasma glycan traits from pre to post-exercise are shown for acute bout of exercise (Acute) and after 21 days (Day 21) in placebo (grey bars) and quercetin (green bars). A) agalactosylation (G0); B) monogalactosylation (G1); C) digalactosylation (G2); D) total galactosylation (Gtotal); E) total sialylation (Stotal); and F) total branching (Btotal). Orange asterisk indicates significant within-subject difference.

Plasma digalactosylation (G2) and total galactosylation (Gtotal), both anti-inflammatory markers, significantly increased post-exercise in placebo (both $p < 0.05$, Figure 7C and 7D), reflecting a transient anti-inflammatory glycomic shift. No significant changes were observed in IgG markers.

GlycanAge

Baseline GlycanAge at study entry ranged from 20 to 74 years across participants, with a mean of 47.8 ± 22.4 years, indicating marked inter-individual heterogeneity in glycan-derived biological ageing. There was a non-significant trend towards increased GlycanAge index post-exercise in placebo, and a non-significant decrease post-exercise in quercetin on day 21 (Figure 8).

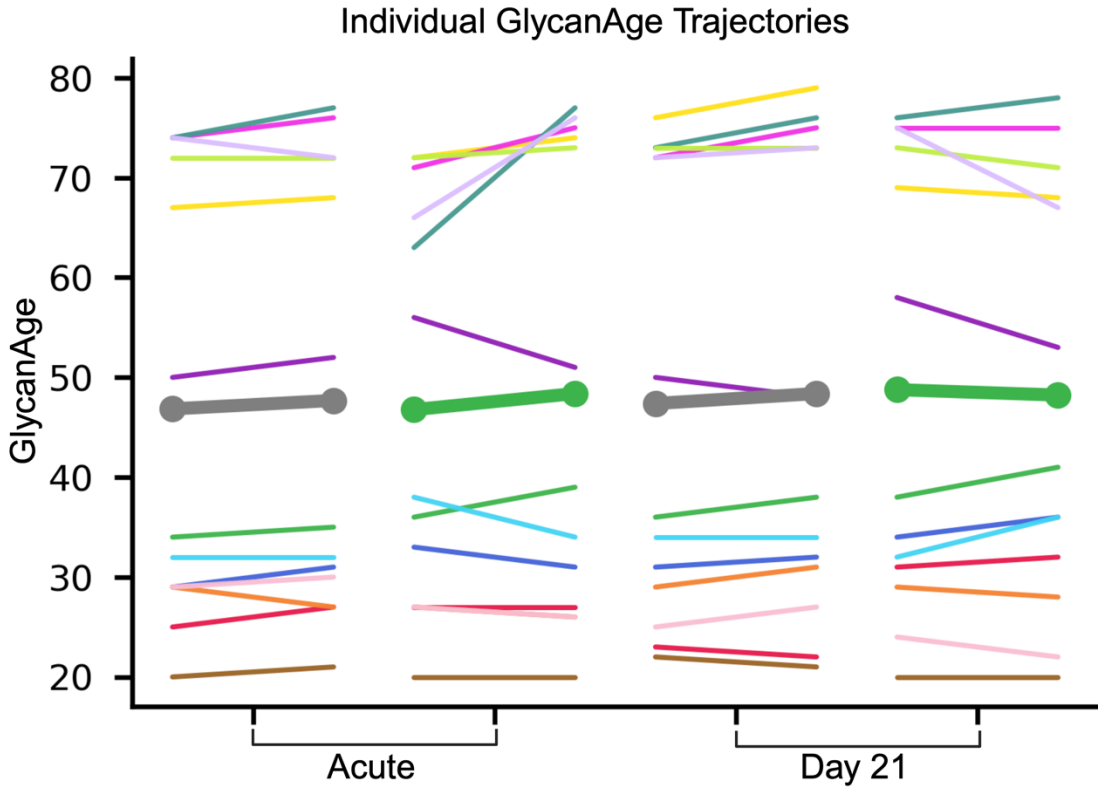

Figure 8. Individual GlycanAge trajectories from pre to post-exercise during acute supplementation (Acute) and short-term (Day 21) supplementation. Thin coloured lines represent within-individual changes for each participant, while bold green and grey lines with end-point markers denote group mean GlycanAge for quercetin (bold green) and placebo (bold grey).

Discussion

The present study investigated the combined and independent effects of HIIE and quercetin supplementation on DNA damage response and inflammation in apparently healthy middle-aged men. The findings provide new insights into how acute HIIE interacts with a bioactive flavonoid to modulate the DNA damage response and post-translational protein glycosylation. By integrating molecular, cellular, and glycomics readouts, this study addresses a gap in current knowledge regarding how nutritional bioactives may potentiate the hormetic adaptations induced by exercise, which are central to genomic maintenance during ageing.

Quercetin Levels and Uptake

Plasma quercetin aglycone concentrations increased in all timepoints in the quercetin group, confirming effective systemic delivery at the administered dose of 1,000 mg/day. Significant elevations were observed after the first dose, which increased linearly following 21 days of continuous intake, consistent with previous reports demonstrating the accumulation of quercetin and its metabolites in plasma over repeated dosing [56-58]. Importantly, super-resolution 3D microscopy demonstrated nuclear localisation of native, unstained quercetin within PBMCs following acute HIIE in all exercise sessions and treatment conditions. At baseline, quercetin fluorescence was predominantly cytoplasmic, whereas post-exercise, discrete nuclear puncta were evident. This observation provides cellular evidence that exercise may facilitate the intracellular trafficking of quercetin, potentially via stress-induced changes in membrane permeability, transporter expression, or nuclear pore activity. Quercetin interacts with multiple uptake and efflux transporters, thereby modulating its absorption and intracellular disposition. In Caco-2 monolayers, quercetin is partly taken up via OATP2B1 (OATP-B) and is actively effluxed by MRP2 [59]. *In vivo*, BCRP (ABCG2) and MRP2 limit net intestinal uptake by apically effluxing quercetin glucuronides, thereby restricting systemic availability [60]. Moreover, under conditions of oxidative or inflammatory stress, the cellular handling of

quercetin may shift. For example, mitochondrial dysfunction in LPS-activated macrophages enhances deconjugation of quercetin glucuronides and leads to greater intracellular accumulation of quercetin aglycone via deconjugation-mediated local release and passive diffusion [61]. Beyond the gut and immune cells, transporter systems in peripheral tissues can themselves be responsive to physiological stimuli such as exercise. An example is GLUT4, a facilitative glucose transporter in skeletal muscle whose expression and membrane translocation are robustly upregulated by exercise [62]. This demonstrates that membrane transport pathways are not static but can adapt to metabolic demands. By analogy, exercise could act as a physiological "adjuvant," potentially modulating transporter or deconjugation systems to enhance the access of bioactives such as quercetin to intracellular and nuclear targets.

DNA Damage

Acute bouts of HIIE elicited an increase in DNA damage as determined by single-strand breaks (alkaline comet assay), oxidised purine bases (FPG-modified comet assay), and double-strand break foci (γH2AX/53BP1 colocalisation). These changes are consistent with prior work demonstrating that intense aerobic exercise increases ROS production through mitochondrial electron transport chain activity, NADPH oxidase activation, and xanthine oxidase flux [63]. Notably, the quercetin arm exhibited significantly lower levels of DNA damage post-exercise compared with placebo—both acutely and after short-term supplementation for double-strand breaks, and after short-term supplementation for single-strand breaks and oxidised purine bases. This pattern likely reflects faster double-strand break resolution and enhanced repair efficiency mediated by quercetin-induced activation of SIRT6 and PARP1, which facilitate chromatin deacetylation, PARP1 recruitment, and repair complex assembly [27,64]. Consequently, fewer γH2AX/53BP1 foci remained at the post-exercise sampling point, consistent with accelerated DNA damage clearance rather than reduced initial lesion formation. Alternatively, the apparent discrepancy between double and single-strand break outcomes may partly arise from the higher sensitivity and spatial resolution of 3D super-resolution microscopy,

which enables detection of subtle chromatin-associated foci that conventional comet-based assays may underestimate.

Quercetin supplementation may attenuate exercise-induced oxidative DNA damage likely through both direct and indirect mechanisms. Quercetin's catechol B-ring (3',4'-dihydroxy groups) and C2–C3 double bond conjugated with a 4-oxo group enable strong electron donation to neutralise superoxide, peroxyl, and hydroxyl radicals [21]. Moreover, quercetin chelates Fe^{2+} and Cu^{2+} ions, thereby inhibiting Fenton-type reactions that otherwise generate hydroxyl radicals capable of cleaving the deoxyribose backbone and causing single- and double-strand breaks [65]. By limiting •OH formation and quenching existing ROS, quercetin also curtails hydroxyl-radical attack on guanine, preventing formation of 8-oxo-7,8-dihydroguanine (8-oxoG), the signature oxidative purine lesion [66]. Beyond radical scavenging, quercetin can modulate cellular redox homeostasis by activating endogenous antioxidant systems, including the Nrf2 pathway and phase II detoxification enzymes [29,30]. Exercise itself is a well-established hormetic stimulus: a transient increase in RONS during exercise can activate redox-sensitive signalling pathways, leading to long-term upregulation of endogenous antioxidant defences and DNA repair enzymes [8,12-14, 67]. The data from this study indicate that quercetin does not blunt this hormetic effect acutely; post-exercise DNA damage markers significantly increased in both treatment groups acutely. However, following 21 days of quercetin supplementation, the magnitude of oxidative DNA damage post-exercise was lower compared to the placebo group. This pattern aligns with a model in which quercetin supports the maintenance of redox balance and genomic stability during a condition of physiological stress, rather than preventing the initial ROS signal entirely.

The significant decrease in DNA double-strand breaks post-exercise is noteworthy, as unresolved double-strand breaks can lead to genomic instability and senescence [68]. The attenuation of double-strand break signalling suggests either reduced initial lesion formation due to quercetin's antioxidant properties or more efficient DNA damage resolution. Quercetin has been shown to activate Nrf2 by promoting its stabilisation and

nuclear translocation, thereby enhancing antioxidant gene expression, and to modulate the DNA repair enzymes PARP1 and SIRT6 by influencing their recruitment and activity at sites of double-strand breaks [25,69].

DNA Repair

SIRT1 expression significantly increased post-exercise in all placebo sessions (Figure 5A), consistent with previous human studies [70]. SIRT1 is a NAD^+-dependent deacetylase that deacetylates p53 to modulate DNA damage-induced cell cycle arrest, deacetylates FOXO transcription factors to upregulate antioxidant genes, and interacts with Ku70 to regulate non-homologous end-joining of DNA breaks [71,72]. Its activation during exercise reflects its role as a metabolic sensor responding to increased AMP/ATP ratios and NAD^+ levels [71,72]. In the quercetin arm, the post-exercise *SIRT1* increase was lost, suggesting a shift toward a more balanced basal redox state with supplementation. Quercetin can increase SIRT1 activity, promote mitochondrial biogenesis, and activate antioxidant pathways in various models [73-75]. The attenuation of post-exercise *SIRT1* increase in quercetin may reflect reduced oxidative and metabolic stress through quercetin's antioxidant and mitochondrial-enhancing effects, attenuating the need for sustained *SIRT1* upregulation. This pattern parallels human skeletal muscle data where six weeks of HIIT lowered SIRT1 protein content by ~20% but increased its deacetylase activity by ~31%, alongside enhanced mitochondrial enzyme activity, indicating a shift toward greater metabolic efficiency and redox balance rather than loss of function [75]. This interpretation is supported by the concomitant reduction in DNA double-strand breaks following exercise with quercetin, consistent with sustained SIRT1-mediated DNA repair activity under a less oxidising cellular milieu.

Meanwhile, *SIRT6* expression significantly decreased post-exercise in all placebo sessions, but increased post-exercise after 21 days of quercetin supplementation (Figure 5B), consistent with a previous study reporting transient *SIRT6* downregulation in skeletal muscle after vigorous exercise [13]. SIRT6 is a chromatin-bound histone deacetylase and mono-ADP-ribosyltransferase critical for double-strand break repair, chromatin stability,

and metabolic homeostasis [76,77]. Quercetin binds allosterically to SIRT6, enhancing its deacetylase activity [27] and promoting deacetylation of H3K9ac and H3K56ac, histone marks that are dynamically regulated during the DNA damage response [76-78]. Post-exercise nuclear colocalisation of quercetin with SIRT6 was consistently higher in the quercetin group across all timepoints, indicating direct post-translational modulation. Under conditions of oxidative stress such as an increase in DNA damage, SIRT6 levels and nuclear localisation decline, leading to impaired chromatin regulation [79,80]. Nevertheless, SIRT6 is rapidly mobilised to sites of DNA double-strand breaks, where it can deacetylate histone H3K9ac and H3K56ac to stabilise chromatin and facilitate NHEJ and HR [76,77]. The reduction in *SIRT6* transcript observed in the present investigation, therefore likely reflects a transient suppression associated with acute stress signalling, while the protein remains functionally active through chromatin recruitment. In support of this interpretation, DNA double-strand breaks were significantly lower post-exercise with quercetin supplementation both acutely and short-term, possibly suggesting that SIRT6-dependent DNA repair and antioxidant pathways remained intact or were even enhanced, potentially through SIRT6-Nrf2 interaction that promotes antioxidant gene expression and mitigates ROS accumulation. However, this mechanistic underpinning is purely speculative and we present no enzymatic antioxidant data to confirm this supposition.

This interplay between SIRT6, chromatin acetylation, and Nrf2 localisation, provides a mechanistic framework for quercetin-exercise interactions. SIRT6 maintains telomeric chromatin integrity by repressing H3K9ac [77] and facilitates PARP1 recruitment and double-strand break repair through mono-ADP-ribosylation [64, 69]. It also regulates subsets of Nrf2 target genes [55]. Nuclear Nrf2 intensity increased post-exercise in all conditions and was significantly higher in the quercetin arm. Quercetin activates the Nrf2/Keap1 pathway [30] and may further enhance Nrf2 signalling via SIRT6 activation of Nrf2 during oxidative stress [55].

SIRT6 also activates PARP1, a key DNA damage sensor that catalyses poly(ADP-ribosyl)ation to recruit repair factors, functions in BER, and cooperates with SIRT6 in double-strand break repair [64]. Mechanistically, SIRT6 mono-ADP-ribosylates and allosterically stimulates PARP1 at DNA lesions, thereby promoting chromatin relaxation and recruitment of XRCC1, POLβ, and LIG3 during BER, as well as facilitating DNA-PK and CtIP loading at DSBs [64,81,82]. In the present study, *PARP1* expression significantly increased post-exercise in all placebo sessions (Figure 5C), reflecting acute DNA-damage sensing and repair activation, whereas this induction was absent in the quercetin arm, consistent with reduced oxidative stress. Quercetin's effects on PARP1 are concentration-dependent: at physiological levels, quercetin does not inhibit PARP1 catalytic activity [83] but may indirectly support repair by preserving NAD^+ availability through partial CD38 inhibition [84] and by enhancing mitochondrial ATP generation via SIRT1/PGC-1α-mediated mitochondrial biogenesis [73]. Collectively, these mechanisms favour an energy-efficient, SIRT6-coordinated DNA-repair response and prevent PARP1-driven NAD^+/ATP depletion under oxidative stress.

OGG1, which excises 8-oxoG lesions during BER [85], significantly decreased post-exercise in all placebo sessions but significantly increased in quercetin in all active treatment sessions (Figure 5D). Acute *OGG1* repression in placebo likely reflects transient oxidative stress-induced transcriptional downregulation previously observed in healthy participants after vigorous exercise [13]. Quercetin may counteract this via Nrf2 activation, as the latter binds and upregulates the OGG1 promoter [85,86]. In rats, quercetin simultaneously increased Nrf2 and OGG1 protein expression while reducing AP sites and 8-oxo-dG [29], and in human epithelial cells, quercetin increased *OGG1* expression while reducing 8-oxo-dG, indicated enhanced BER [88]. This Nrf2-OGG1 axis likely contributes to sustained DNA repair capacity with supplementation. This is supported by the increases in plasma and nuclear levels of quercetin and Nrf2, as well as the decreased oxidative damage in the current study.

RAD51, a central recombinase mediating HR, catalyses the homology search and strand invasion required for accurate double-strand break repair [89]. In the present study, *RAD51*, *SIRT1*, and *PARP1* all significantly increased post-exercise in the placebo sessions, indicating activation of an oxidative stress-induced repair response. Both SIRT1 and PARP1 are NAD^+-dependent DNA-damage sensors that deacetylate or PARylate chromatin proteins to promote accessibility and initiate ATM/CHK1-dependent double-strand break signalling [90,91]. These upstream events facilitate the recruitment and activation of RAD51 and other HR factors to complete strand invasion and template-guided repair [92,93]. This pattern reflects a canonical DNA damage response cascade, in which oxidative stress triggers PARP1/SIRT1 activation followed by RAD51-mediated HR. In contrast, this induction was absent with quercetin, consistent with quercetin's antioxidant and NAD^+-preserving effects, which reduce lesion burden and thereby diminish the need for HR activation.

Conversely, *SIRT6* and *OGG1* expression significantly declined post-exercise in the placebo group but remained stable in quercetin-supplemented participants. SIRT6 functions as a chromatin-bound sensor of DNA damage that deacetylates H3K9ac and H3K56ac, facilitating chromatin compaction and recruitment of BER enzymes such as OGG1 and APE1 to oxidised guanine residues [64,76]. Under oxidative stress, SIRT6 also mono-ADP-ribosylates and activates PARP1, linking DNA repair to NAD^+ metabolism [64]. Excessive PARP1 activation during oxidative insult causes rapid NAD^+ and ATP depletion, suppressing energy-dependent repair and compromising cell survival [94,95]. The post-exercise decline of *SIRT6* and *OGG1* in placebo therefore indicates a transient impairment of BER capacity consistent with NAD^+ exhaustion and PARP1 overactivation. In contrast, quercetin preserved *SIRT6* and *OGG1* expression, implying sustained chromatin-associated BER efficiency through its antioxidant, NAD^+-sparing (via CD38 inhibition), and SIRT6-activating actions [21,27,96]. Collectively, these findings suggest that in placebo, there was a transient BER suppression and compensatory activation of energy-intensive SIRT1/PARP1-dependent HR, whereas in quercetin, there was a maintenance of energy-efficient SIRT6–OGG1-coordinated BER pathway, preserving redox balance. RAD51-

mediated HR is slower and more ATP-demanding than NHEJ, indicating that quercetin's maintenance of BER favours a rapid and metabolically economical repair response [93].

Glycomic Profiling of IgG and Plasma Proteins

Glycosylation of plasma proteins and immunoglobulins is a sensitive marker of systemic inflammation, metabolic status, and biological ageing [48,98]. Pro-inflammatory glycan traits, including increased agalactosylation (G0), asialylation (S0), and bisecting GlcNAc (B), are associated with chronic low-grade inflammation and immunosenescence, while increased galactosylation (G2, Gtotal) and mono and di-sialylation (S1, S2) are consistently linked to a younger, anti-inflammatory glycan phenotype [48,98-100]. High-intensity exercise elicits transient inflammatory and stress-related signalling, including elevations in cytokines such as IL-6 and TNF-α, which have been shown to influence B cell activation and glycosyltransferase regulation, thereby biasing IgG glycosylation toward agalactosylated and asialylated forms [101–104]. Upstream regulators of genomic stability, including SIRT6, Nrf2, and DNA repair pathways such as base excision repair (BER) and homologous recombination (HR), can attenuate these shifts by limiting persistent DNA damage signalling and NF-κB-mediated cytokine production [105–107]. By enhancing DNA repair capacity and antioxidant defence, these pathways dampen inflammatory signalling and indirectly stabilise the glycome, reducing the emergence of pro-inflammatory glycan traits.

In the current study, plasma galactosylation exhibited a rapid anti-inflammatory shift immediately following exercise, with a significant reduction in G0 and concomitant increases in G2 and Gtotal in placebo, but not in quercetin (Figure 7). Together, these findings suggest that acute post-exercise plasma glycan remodelling reflects a balance between transient immune activation and rapid anti-inflammatory resolution, capturing the tight coupling between oxidative stress, redox homeostasis, and glycosylation dynamics during recovery. Mechanistically, oxidative stress perturbs endoplasmic reticulum and Golgi function by altering organellar redox balance, enzyme activity, and the availability and transport of sugar-nucleotide donors such as UDP-galactose required

for terminal galactosylation [108-110]. RONS can disrupt disulfide bond formation, Golgi pH, and nucleotide-sugar transport, thereby modulating glycosyltransferase activity within the secretory pathway [110-113]. Activation of antioxidant and redox-restorative pathways in the quercetin arm is therefore likely to re-establish metabolic and redox equilibria, stabilising the plasma glycome and limiting the emergence of pro-inflammatory glycan traits.

There was a non-significant trend towards increased GlycanAge index post-exercise in placebo and a non-significant decrease post-exercise after 21 days of quercetin supplementation (Figure 8). Although these effects did not reach statistical significance, the direction of change aligns with the transient oxidative stress induced by acute HIIE and the potential antioxidant influence of quercetin. Quercetin activates Nrf2-dependent antioxidant pathways and suppresses NF-κB signaling [22,25,29,30], mechanisms that could favour restoration of youthful glycan structures over time. However, the 21-day supplementation period may not have been sufficient to elicit measurable GlycanAge improvement, as previous interventions reporting significant reductions typically required several months of sustained dietary or lifestyle modification [114,115].

Conclusion

This study demonstrates that HIIE induces transient oxidative DNA damage and dynamic changes in plasma glycosylation, establishing it as a robust physiological model of acute oxidative stress. Concurrent quercetin supplementation modulated these responses in a manner consistent with improved redox homeostasis and sustained DNA repair capacity. Quercetin uptake was confirmed both systemically and at the cellular level, with nuclear localisation in PBMCs indicating direct access to genomic targets. Supplementation attenuated post-exercise DNA damage, including double and single-strand breaks and oxidised purine bases, while preserving *SIRT6* and *OGG1* expression, supporting maintenance of base excision and chromatin-associated repair pathways, potentially via SIRT6-Nrf2-dependent mechanisms.

In parallel, acute post-exercise plasma glycan remodelling—characterised by reduced agalactosylation and increased galactosylation—was observed in the placebo condition but not with quercetin supplementation, suggesting a stabilisation of glycosylation dynamics under oxidative stress with quercetin. Although changes in the GlycanAge index did not reach statistical significance, the opposing directional trends observed post-exercise in placebo and following short-term quercetin supplementation are consistent with modulation of glycosylation under redox challenge. The lack of statistical significance likely reflects the short intervention period, as glycomic and biological age adaptations generally require sustained modulation. Collectively, these findings position HIIE as a controlled oxidative stress challenge and quercetin as a nutritional co-factor supporting genomic stability and redox balance during acute physiological stress.

Author Contributions

Investigation & Formal Analysis: C.G.J.; Formal Analysis & Resources: N.S.B., F.V.Z.; Supervision: G.D., K.M.

Declaration of Competing Interest

The authors declare that they have no known competing financial interests or personal relationships that could have appeared to influence the work reported in this paper. NSB is an employee of Genos Glycoscience Research Laboratory Ltd and GlycanAge Ltd.

Acknowledgements

The authors thank Genos Ltd. (Zagreb, Croatia) for performing the glycomics profiling of IgG and plasma proteins.

Funding

We are grateful to DoNotAge.org for supplying quercetin aglycone and supporting all LC-MS/MS analyses.

Data Availability Statement

The data that support the findings of this study are available from the corresponding author upon reasonable request.

Supplementary Materials

Supplementary Table S1. Haemoglobin, haematocrit, and estimated plasma volume changes before and after acute exercise. HB haemoglobin; HT haematocrit; P participant.

P	HB Pre-exercise	HB Post-exercise	HT Pre-exercise	HT Post-exercise	%Δ Plasma Volume	%Δ HB	%Δ HT
1							
	15.9	14.2	45	47	7.900128041	-10.6918239	4.444444444
	16.7	17.2	47	48	-4.738920579	2.994011976	2.127659574
	15.8	15.7	48	50	-3.233708966	-0.632911392	4.166666667
	15.6	16	47	51	-9.858490566	2.564102564	8.510638298
2							
	13.6	13.8	43	44	-3.178235444	1.470588235	2.325581395
	13.8	17.1	43	45	-22.12988612	23.91304348	4.651162791
	15.7	15.2	46	44	7.115009747	-3.184713376	-4.347826087
	13.3	13.9	46	44	-0.772715161	4.511278195	-4.347826087
3							
	17.2	16.7	44	51	-9.880239521	-2.906976744	15.90909091
	15.8	15.7	42	49	-11.50889523	-0.632911392	16.66666667
	14.2	15.2	42	48	-16.24319419	7.042253521	14.28571429
	13.8	17.1	46	49	-23.78167641	23.91304348	6.52173913
4							
	15.8	15.7	44	46	-2.957233849	-0.632911392	4.545454545

	15.8	16.7	44	47	-10.45765612	5.696202532	6.818181818
	15.2	15.7	43	48	-11.67728238	3.289473684	11.62790698
	14.3	14.7	46	47	-4.522549761	2.797202797	2.173913043
5							
	14.7	13.8	43	46	0.915331808	-6.12244898	6.976744186
	14.9	15	44	46	-4.214285714	0.67114094	4.545454545
	14.1	14	43	44	-1.052631579	-0.709219858	2.325581395
	17.1	16	44	41	12.60044643	-6.432748538	-6.818181818
6							
	13.7	14.5	41	42	-7.118644068	5.839416058	2.43902439
	14.9	13.9	42	41	9.042421235	-6.711409396	-2.380952381
	12.2	14.2	41	40	-12.62831225	16.39344262	-2.43902439
	12.8	15.8	38	41	-22.90730911	23.4375	7.894736842
7							
	13.8	13.9	47.5	45.5	3.062692703	0.724637681	-4.210526316
	14.9	15	47	45	3.081761006	0.67114094	-4.255319149
	12.2	14.2	47	46	-12.46346001	16.39344262	-2.127659574
	15	16.1	47	46	-5.074416969	7.333333333	-2.127659574
8							
	13.3	13.9	45	47	-7.795945062	4.511278195	4.444444444
	13.9	13.7	44	43	3.271637122	-1.438848921	-2.272727273
	12.1	12.1	44	46	-3.571428571	0	4.545454545

	16.3	15.5	48	48	5.161290323	-4.90797546	0
9							
	15.1	14.9	42	44	-2.152279565	-1.324503311	4.761904762
	15.8	14.1	40	42	8.321513002	-10.75949367	5
	14.3	12.8	42	44	7.86637931	-10.48951049	4.761904762
	14.6	14.8	44	45	-3.112934363	1.369863014	2.272727273
10							
	14.9	15	44	43	1.107142857	0.67114094	-2.272727273
	13.5	13.2	41	39	5.739599384	-2.222222222	-4.87804878
	13.2	13.3	43	42	0.989315394	0.757575758	-2.325581395
	15.3	13	41	43	13.70273794	-15.03267974	4.87804878
11							
	14.9	14.5	45	47	-0.978056426	-2.684563758	4.444444444
	13.6	15.7	46	47	-14.9799481	15.44117647	2.173913043
	13.2	15.6	48	46	-12.13017751	18.18181818	-4.166666667
	13	15.2	43	46	-18.97506925	16.92307692	6.976744186
12							
	13	14.1	44	41	-2.862208713	8.461538462	-6.818181818
	14.1	12.8	44	43	12.12332589	-9.219858156	-2.272727273
	12.9	14	46	43	-2.738095238	8.527131783	-6.52173913
	13	11.6	43	41.5	15.01814882	-10.76923077	-3.488372093

13							
	14.7	16.4	54	48	1.325556734	11.56462585	-11.11111111
	11.6	12.4	49	48	-4.617330803	6.896551724	-2.040816327
	11.6	12.4	52	48	1.344086022	6.896551724	-7.692307692
	11.6	12.4	48	50	-10.04962779	6.896551724	4.166666667

Supplementary Table S2A. The glycan structures corresponding to each of the glycan peaks (GP) are shown. In the case of multiple structures per glycan peak, the upper structure is the major one, and the lower one is minor in abundance.

Peak #	**Structure**	**Composition**	**Ratio of coeluted structures**
GP1	FA2	H3N4F1	
GP2	FA2B	H3N5F1	major structure
	M5	H5N2	low abundance
GP3	A2BG1	H4N5	
GP4	FA2[6]G1	H4N4F1	
GP5	FA2[3]G1	H4N4F1	
GP6	FA2[6]BG1	H4N5F1	
GP7	M6	H6N2	major structure
	FA2[3]BG1	H4N5F1	low abundance
GP8	A2G2	H5N4	
GP9	A2BG2	H5N5	
GP10	FA2G2	H5N4F1	
GP11	FA2BG2	H5N5F	
GP12	M7	H7N2	major structure
	A2G2S1	H5N4S1	major structure
	A1M4G1S1	H5N3S1	low abundance
	A2BG1S1	H4N5S1	low abundance
GP13	FA2G1S1	H4N4F1S1	major structure
	FA2BG1S1	H4N5F1S1	low abundance
GP14	A2G2S1	H5N4S1	
GP15	A2BG2S1	H5N5S1	
GP16	FA2G2S1	H5N4F1S1	
GP17	FA2BG2S1	H5N5F1S1	
GP18	A2G2S2	H5N4S2	major structure
	FA2G2S2	H5N4F1S2	low abundance

GP19	M9	H9N2	
GP20	A2G2S2	H5N4S2	
GP21	A2G2S2	H5N4S2	major structure
	A3G3S1	H6N5S1	low abundance
	FA2G2S2	H5N4F1S2	low abundance
	A2BG2S2	H5N5S2	low abundance
	A3F1G3S1	H6N5F1S1	low abundance
GP22	FA2G2S2	H5N4F1S2	
GP23	FA2BG2S2	H5N5F1S2	
GP24	A3G3S2	H6N5S2	major structure
	A3F1G3S1	H6N5F1S1	low abundance
GP25	A3G3S2	H6N5S2	major structure
	FA2F1G2S2	H5N4F2S2	low abundance

	A3F1G3S2	H6N5F1S2	low abundance
GP26	A3G3S2	H6N5S2	major structure
	FA3G3S2	H6N5F1S2	low abundance
GP27	A3F1G3S2	H6N5F1S2	major structure
	A3G3S3	H6N5S3	low abundance
GP28	A3G3S3	H6N5S3	major structure
	A3F1G3S2	H6N5F1S2	low abundance
GP29	A3G3S3	H6N5S3	major structure
	A3F1G3S2	H6N5F1S2	low abundance
GP30	A3G3S3	H6N5S3	major structure
	A3F1G3S3	H6N5F1S3	low abundance
GP31	FA3G3S3	H6N5F1S3	major structure
	A3G3S3	H6N5S3	low abundance
GP32	A3G3S3	H6N5S3	
GP33	A3F1G3S3	H6N5F1S3	
GP34	FA3G3S3	H6N5F1S3	major structure
	A4G4S3	H7N6S3	low abundance
GP35	FA3F1G3S3	H6N5F2S3	major structure
	A4F1G4S3	H7N6F1S3	low abundance
GP36	A4G4S3	H7N6S3	major structure
	A4F1G4S3	H7N6F1S3	low abundance
GP37	A4G4S4	H7N6S4	major structure
	A4F1G4S3	H7N6F1S3	low abundance
GP38	A4G4S4	H7N6S4	major structure
	A4F1G4S4	H7N6F1S4	low abundance
	A4F1G4S3	H7N6F1S3	low abundance
GP39	A4F1G4S4	H7N6F1S4	major structure
	A4F2G4S4	H7N6F2S4	low abundance

Supplementary Table S2B. The glycan structures corresponding to each of the IgG glycan peaks in CGE (P) are shown.

Peak	Glycan structure	Composition
P1	A2G2S2	H5N4S2
P2	A2BG2S2	H5N5S2
P3	FA2G2S2	H5N4F1S2
P4	FA2BG2S2	H5N5F1S2
P5	A2[6]G1S1	H4N4S1
P6	A2[3]G1S1	H4N4S1
P7	FA2[6]G1S1	H4N4F1S1
P8	FA2[3]G1S1	H4N4F1S1
P9	A2G2[6]S1	H5N4S1
P10	A2G2[3]S1	H5N4S1
P11	A2BG2S1	H5N5S1
P12	FA2G2S1, M5, A2	H5N4F1S1
P13	FA2BG2S1	H5N5F1S1
P14	A2B	H3N5
P15	FA2	H3N4F1
P16	A2[6]G1	H4N4
P17	A2[3]G1	H4N4
P18	FA2B	H3N5F1
P19	A2B[6]G1	H4N5
P20	A2B[3]G1	H4N5
P21	FA2[6]G1	H4N4F1
P22	FA2[3]G1	H4N4F1
P23	FA2B[6]G1, A2G2	H4N5F1
P24	FA2B[3]G1	H4N5F1
P25	A2BG2	H5N5
P26	FA2G2	H5N4F1
P27	FA2BG2	H5N5F

Supplementary Table S3. Plasma glycan changes from pre to post-exercise in all participants (n = 13). P placebo; Q quercetin; PRE pre-exercise; POS post-exercise; Bonf Bonferroni; log log-transformed

Glycan Trait	Pair	PRE mean	POS mean	Delta POS minus PRE	t	p raw	p Bonf
Btotal	Day21-P	11.7826377	11.668227	-0.114410769	0.262514	0.797378	1
Btotal	Day21-Q	12.50274	12.017218	-0.485522308	1.441841	0.174933	0.349865554
Btotal	Day1-P	12.1972646	12.054622	-0.142643077	0.934569	0.368436	0.736871942
Btotal	Day1-Q	11.8097946	11.747184	-0.062610769	0.582852	0.570784	1
G0 (log)	Day21-P	1.81951403	1.9014443	0.081930246	-1.72225	0.110673	0.221345406
G0 (log)	Day21-Q	1.94577222	1.9434415	-0.002330727	0.11765	0.908292	1
G0 (log)	**Day1-P**	**1.94849571**	**1.9111734**	**-0.03732229**	**2.677706**	**0.020122**	**0.040244181**
G0 (log)	Day1-Q	1.90651046	1.909552	0.003041533	-0.21467	0.833632	1
G1	Day21-P	9.66685	10.312916	0.646066154	-1.60576	0.134304	0.26860884
G1	Day21-Q	10.5681185	10.660586	0.092467692	-0.38825	0.704632	1
G1	Day1-P	10.8011369	10.480288	-0.320849231	2.272959	0.042212	0.084423719
G1	Day1-Q	10.4447092	10.468203	0.023493846	-0.1476	0.885108	1
G2	Day21-P	56.8133785	54.996632	-1.816746923	2.250733	0.043939	0.087878223
G2	Day21-Q	55.3154885	55.27879	-0.036698462	0.064035	0.949997	1
G2	**Day1-P**	**54.74987**	**55.844888**	**1.095017692**	**-4.07702**	**0.001534**	**0.003068353**
G2	Day1-Q	55.1573838	55.071235	-0.086148462	0.266198	0.794606	1
Gtotal	Day21-P	86.7290931	86.103265	-0.625828462	1.861327	0.087363	0.174725993
Gtotal	Day21-Q	85.9912708	85.983824	-0.007446923	0.040886	0.968059	1
Gtotal	**Day1-P**	**85.9320231**	**86.248942**	**0.316919231**	**-3.1114**	**0.008997**	**0.017994801**
Gtotal	Day1-Q	86.18661	86.122056	-0.064553846	0.532988	0.603773	1
Stotal	Day21-P	72.6244623	71.202915	-1.421546923	1.690574	0.116704	0.233408564
Stotal	Day21-Q	70.5947631	70.540032	-0.054730769	0.120362	0.906188	1
Stotal	Day1-P	70.3690654	70.969118	0.600052308	-2.40729	0.033076	0.066151975

Stotal	Day1-Q	71.0644254	70.995362	-0.069063846	0.238762	0.815319	1

References

1. Sies H. Oxidative stress: a concept in redox biology and medicine. Redox Biol. 2015;4:180-3. doi: 10.1016/j.redox.2015.01.002. Epub 2015 Jan 3. PMID: 25588755; PMCID: PMC4309861.
2. Lindahl T. Instability and decay of the primary structure of DNA. Nature. 1993 Apr 22;362(6422):709-15. doi: 10.1038/362709a0.
3. David SS, O'Shea VL, Kundu S. Base-excision repair of oxidative DNA damage. Nature. 2007 Jun 21;447(7147):941-50. doi: 10.1038/nature05978.
4. Ciccia A, Elledge SJ. The DNA damage response: making it safe to play with knives. Mol Cell. 2010 Oct 22;40(2):179-204. doi: 10.1016/j.molcel.2010.09.019.
5. Wallace SS. Base excision repair: a critical player in many games. DNA Repair (Amst). 2014 Jul;19:14-26. doi: 10.1016/j.dnarep.2014.03.030.
6. López-Otín C, Blasco MA, Partridge L, Serrano M, Kroemer G. The hallmarks of aging. Cell. 2013 Jun 6;153(6):1194-217. doi: 10.1016/j.cell.2013.05.039.
7. Gorbunova V, Seluanov A, Mao Z, Hine C. Changes in DNA repair during aging. Nucleic Acids Res. 2007;35(22):7466-74. doi: 10.1093/nar/gkm756.
8. Ji LL. Antioxidant signaling in skeletal muscle: a brief review. Exp Gerontol. 2007 Jul;42(7):582-93. doi: 10.1016/j.exger.2007.03.002.
9. Powers SK, Radak Z, Ji LL. Exercise-induced oxidative stress: past, present and future. J Physiol. 2016 Sep 15;594(18):5081-92. doi: 10.1113/JP270646.
10. Tryfidou DV, McClean C, Nikolaidis MG, Davison GW. DNA Damage Following Acute Aerobic Exercise: A Systematic Review and Meta-analysis. Sports Med. 2020 Jan;50(1):103-127. doi: 10.1007/s40279-019-01181-y.
11. Soares JP, Silva AM, Oliveira MM et al. Effects of combined physical exercise training on DNA damage and repair capacity: role of oxidative stress changes. Age (Dordr). 2015 Jun;37(3):9799. doi: 10.1007/s11357-015-9799-4.
12. Gomez-Cabrera MC, Domenech E, Viña J. Moderate exercise is an antioxidant: upregulation of antioxidant genes by training. Free Radic Biol Med. 2008 Jan 15;44(2):126-31. doi: 10.1016/j.freeradbiomed.2007.02.001.
13. Radak Z, Bori Z, Koltai E et al. Age-dependent changes in 8-oxoguanine-DNA glycosylase activity are modulated by adaptive responses to physical exercise in human skeletal muscle. Free Radic Biol Med. 2011 Jul 15;51(2):417-23. doi: 10.1016/j.freeradbiomed.2011.04.018.
14. Radak Z, Chung HY, Goto S. Systemic adaptation to oxidative challenge induced by regular exercise. Free Radic Biol Med. 2008 Jan 15;44(2):153-9. doi: 10.1016/j.freeradbiomed.2007.01.029.
15. Muthusamy VR, Kannan S, Sadhaasivam K et al. Acute exercise stress activates Nrf2/ARE signaling and promotes antioxidant mechanisms in the myocardium. Free Radic Biol Med. 2012 Jan 15;52(2):366-76. doi: 10.1016/j.freeradbiomed.2011.10.440.
16. Kang C, Li Ji L. Role of PGC-1α signaling in skeletal muscle health and disease. Ann N Y Acad Sci. 2012 Oct;1271(1):110-7. doi: 10.1111/j.1749-6632.2012.06738.x.
17. Cash SW, Beresford SA, Vaughan TL et al. Recent physical activity in relation to DNA damage and repair using the comet assay. J Phys Act Health. 2014 May;11(4):770-6. doi: 10.1123/jpah.2012-0278.

18. Denham J, O'Brien BJ, Harvey JT et al. Genome-wide sperm DNA methylation changes after 3 months of endurance training in humans. Epigenomics. 2015;7(5):717-731. doi:10.2217/epi.15.29. PMID: 26111106.

19. Kawakami R, Kashino I, Kasai H et al. Leisure-time physical activity and DNA damage among Japanese workers. PLoS One. 2019 Feb 15;14(2):e0212499. doi: 10.1371/journal.pone.0212499.

20. Santovito A, Agostinovna Nigretti A et al. Regular Sport Activity Is Able to Reduce the Level of Genomic Damage. Biology (Basel). 2023 Aug 9;12(8):1110. doi: 10.3390/biology12081110.

21. Boots AW, Haenen GR, Bast A. Health effects of quercetin: from antioxidant to nutraceutical. Eur J Pharmacol. 2008 May 13;585(2-3):325-37. doi: 10.1016/j.ejphar.2008.03.008.

22. Zhang F, Feng J, Zhang J et al. Quercetin modulates AMPK/SIRT1/NF-κB signaling to inhibit inflammatory/oxidative stress responses in diabetic high fat diet-induced atherosclerosis in the rat carotid artery. Exp Ther Med. 2020 Dec;20(6):280. doi: 10.3892/etm.2020.9410.

23. Lu Z, Wang H, Ishfaq M, Han Y, Zhang X, Li X, Wang B, Lu X, Gao B. Quercetin and AMPK: A Dynamic Duo in Alleviating MG-Induced Inflammation via the AMPK/SIRT1/NF-κB Pathway. Molecules. 2023 Nov 2;28(21):7388. doi: 10.3390/molecules28217388.

24. Cui Z, Zhao X, Amevor FK, Du X, Wang Y, Li D, Shu G, Tian Y, Zhao X. Therapeutic application of quercetin in aging-related diseases: SIRT1 as a potential mechanism. Front Immunol. 2022 Jul 22;13:943321. doi: 10.3389/fimmu.2022.943321.

25. Abd El-Emam MM, Mostafa M, Farag AA et al. The Potential Effects of Quercetin-Loaded Nanoliposomes on Amoxicillin/Clavulanate-Induced Hepatic Damage: Targeting the SIRT1/Nrf2/NF-κB Signaling Pathway and Microbiota Modulation. Antioxidants (Basel). 2023 Jul 25;12(8):1487. doi: 10.3390/antiox12081487.

26. Tanigawa S, Fujii M, Hou DX. Action of Nrf2 and Keap1 in ARE-mediated NQO1 expression by quercetin. Free Radic Biol Med. 2007 Jun 1;42(11):1690-703. doi: 10.1016/j.freeradbiomed.2007.02.017.

27. You W, Zheng W, Weiss S et al. Structural basis for the activation and inhibition of Sirtuin 6 by quercetin and its derivatives. Sci Rep. 2019 Dec 16;9(1):19176. doi: 10.1038/s41598-019-55654-1.

28. Rahnasto-Rilla M, Tyni J, Huovinen M et al. Natural polyphenols as sirtuin 6 modulators. Sci Rep. 2018 Mar 7;8(1):4163. doi: 10.1038/s41598-018-22388-5.

29. Darband SG, Sadighparvar S, Yousefi B, Kaviani M, Ghaderi-Pakdel F, Mihanfar A, Rahimi Y, Mobaraki K, Majidinia M. Quercetin attenuated oxidative DNA damage through NRF2 signaling pathway in rats with DMH induced colon carcinogenesis. Life Sci. 2020 Jul 15;253:117584. doi: 10.1016/j.lfs.2020.117584.

30. Yousefi Zardak M, Keshavarz F, Mahyaei A, Gholami M et al. Quercetin as a therapeutic agent activate the Nrf2/Keap1 pathway to alleviate lung ischemia-reperfusion injury. Sci Rep. 2024 Oct 4;14(1):23074. doi: 10.1038/s41598-024-73075-7.

31. Ansar S, Siddiqi NJ, Zargar S, Ganaie MA, Abudawood M. Hepatoprotective effect of Quercetin supplementation against Acrylamide-induced DNA damage in wistar rats. BMC Complement Altern Med. 2016 Aug 30;16(1):327. doi: 10.1186/s12906-016-1322-7.

32. Hussain Y, Abdullah, Khan F et al. Role of Quercetin in DNA Repair: Possible Target to Combat Drug Resistance in Diabetes. Curr Drug Targets. 2024;25(10):670-682. doi: 10.2174/0113894501302098240430164446.

33. Bujarrabal-Dueso A, Garinis GA, Robbins PD et al. Targeting DNA damage in ageing: towards supercharging DNA repair. Nat Rev Drug Discov. 2025 Oct;24(10):785-807. doi: 10.1038/s41573-025-01212-6.

34. Graefe EU, Wittig J, Mueller S et al. Pharmacokinetics and bioavailability of quercetin glycosides in humans. J Clin Pharmacol. 2001 May;41(5):492-9. doi: 10.1177/00912700122010366.

35. European Medicines Agency (EMA). Guideline on the Investigation of Bioequivalence (Rev 1) — CPMP/EWP/QWP/1401/98 Rev 1. London: EMA; 20 January 2010. Available at: https://www.ema.europa.eu/en/documents/scientific-guideline/guideline-investigation-bioequivalence-rev1_en.pdf

36. Dill DB, Costill DL. Calculation of percentage changes in volumes of blood, plasma, and red cells in dehydration. J Appl Physiol. 1974;37(2):247-248.

37. Ammar A, Chtourou H, Trabelsi K et al. Temporal specificity of training: intra-day effects on biochemical responses and Olympic-Weightlifting performances. J Sports Sci. 2015;33(4):358-68. doi: 10.1080/02640414.2014.944559.

38. Yang LL, Xiao N, Li XW et al. Pharmacokinetic comparison between quercetin and quercetin 3-O-β-glucuronide in rats by UHPLC-MS/MS. Sci Rep. 2016 Oct 24;6:35460. doi: 10.1038/srep35460.

39. Drummond NJ, Davies NO, Lovett JE et al. A synthetic cell permeable antioxidant protects neurons against acute oxidative stress. Sci Rep. 2017 Sep 19;7(1):11857. doi: 10.1038/s41598-017-12072-5.

40. Pan H, Guan D, Liu X et al. SIRT6 safeguards human mesenchymal stem cells from oxidative stress by coactivating NRF2. Cell Res. 2016 Feb;26(2):190-205. doi: 10.1038/cr.2016.4.

41. Pradhan AK, Shi Q, Tartler KJ, Rammes G. Quantification of astrocytic synaptic pruning in mouse hippocampal slices in response to ex vivo Aβ treatment via colocalization analysis with C1q. STAR Protoc. 2022 Dec 16;3(4):101687. doi: 10.1016/j.xpro.2022.101687.

42. Collins A, Møller P, Gajski G et al. Measuring DNA modifications with the comet assay: a compendium of protocols. Nat Protoc. 2023 Mar;18(3):929-989. doi: 10.1038/s41596-022-00754-y.

43. Jezkova L, Zadneprianetc M, Kulikova EA, et al. Particles with similar LET values generate DNA breaks of different complexity and reparability: a high-resolution microscopy analysis of γH2AX/53BP1 foci. Nanoscale. 2018;10(35):16587-16597. doi:10.1039/c8nr06829h

44. Ruprecht N, Hungerbühler MN, Böhm IB, Heverhagen JT. Improved identification of DNA double strand breaks: γ-H2AX-epitope visualization by confocal microscopy and 3D reconstructed images. Radiation and Environmental Biophysics. 2019;58(2):295-302. doi:10.1007/s00411-019-00778-1

45. Hanić M, Lauc G, Trbojević-Akmačić I. N-Glycan Analysis by Ultra-Performance Liquid Chromatography and Capillary Gel Electrophoresis with Fluorescent Labeling. Curr Protoc Protein Sci. 2019 Sep;97(1):e95. doi: 10.1002/cpps.95.

46. Ruhaak LR, Hennig R, Huhn C et al. Optimized workflow for preparation of APTS-labeled N-glycans allowing high-throughput analysis of human plasma glycomes using 48-channel multiplexed CGE-LIF. J Proteome Res. 2010 Dec 3;9(12):6655-64. doi: 10.1021/pr100802f.

47. Shkunnikova S, Mijakovac A, Sironic L et al. IgG glycans in health and disease: Prediction, intervention, prognosis, and therapy. Biotechnol Adv. 2023 Oct;67:108169. doi: 10.1016/j.biotechadv.2023.108169.

48. Krištić J, Vučković F, Menni C, Klarić L, Keser T, Beceheli I, et al. Glycans are a novel biomarker of chronological and biological ages. J Gerontol A Biol Sci Med Sci. 2014;69(7):779-789. doi:10.1093/gerona/glt190.

49. López-Otín C, Blasco MA, Partridge L, Serrano M, Kroemer G. Hallmarks of aging: An expanding universe. Cell. 2023 Jan 19;186(2):243-278. doi: 10.1016/j.cell.2022.11.00

50. Jurić J, Kohrt WM, Kifer D, Gavin KM, Pezer M, Nigrovic PA, Lauc G. Effects of estradiol on biological age measured using the glycan age index. Aging (Albany NY). 2020 Oct 13;12(19):19756-19765. doi: 10.18632/aging.104060.

51. Rapčan B, Song M, Frkatović-Hodžić A et al. Glycan clock of ageing-analytical precision and time-dependent inter- and i-individual variability. Geroscience. 2024 Dec;46(6):5781-5796. doi: 10.1007/s11357-024-01239-4. Epub 2024 Jun 14. PMID: 38877341; PMCID: PMC

52. Fogarty MC, Hughes CM, Burke G, Brown JC, Davison GW. Acute and chronic watercress supplementation attenuates exercise-induced peripheral mononuclear cell DNA damage and lipid peroxidation. Br J Nutr. 2013 Jan 28;109(2):293-301. doi: 10.1017/S0007114512000992.

53. International Council for Harmonisation (ICH). Statistical Principles for Clinical Trials (E9). Geneva: ICH; 1998. Available from: https://www.ema.europa.eu/en/ich-e9-statistical-principles-clinical-trials-scientific-guideline

54. Dmitrienko A, Wiens BL, Tamhane AC et al. Tree-structured gatekeeping tests in clinical trials with hierarchically ordered multiple objectives. Stat Med. 2007 May 30;26(12):2465-78. doi: 10.1002/sim.2716.

55. Rezazadeh S, Yang D, Tombline G, Simon M, Regan SP, Seluanov A, Gorbunova V. SIRT6 promotes transcription of a subset of NRF2 targets by mono-ADP-ribosylating BAF170. Nucleic Acids Res. 2019 Sep 5;47(15):7914-7928. doi: 10.1093/nar/gkz528.

56. Burak C, Brüll V, Langguth P et al. Higher plasma quercetin levels following oral administration of an onion skin extract compared with pure quercetin dihydrate in humans. Eur J Nutr. 2017 Feb;56(1):343-353. doi: 10.1007/s00394-015-1084-x.

57. Egert S, Wolffram S, Bosy-Westphal A, Boesch-Saadatmandi C, Wagner AE, Frank J, Rimbach G, Mueller MJ. Daily quercetin supplementation dose-dependently increases plasma quercetin concentrations in healthy humans. J Nutr. 2008 Sep;138(9):1615-21. doi: 10.1093/jn/138.9.1615.

58. Moon YJ, Wang L, DiCenzo R et al. Quercetin pharmacokinetics in humans. Biopharm Drug Dispos. 2008 May;29(4):205-17. doi: 10.1002/bdd.605.

59. Chabane M, Al Ahmad A, Peluso J et al. Quercetin and naringenin transport across human intestinal Caco-2 cells. J Pharm Pharmacol. 2009 Nov;61(11):1473-83. doi: 10.1211/jpp/61.11.0006.

60. Sesink AL, Arts IC, de Boer VC et al. Breast cancer resistance protein (Bcrp1/Abcg2) limits net intestinal uptake of quercetin in rats by facilitating apical efflux of glucuronides. Mol Pharmacol. 2005 Jun;67(6):1999-2006. doi: 10.1124/mol.104.009753.

61. Ishisaka A, Kawabata K, Miki S et al. Mitochondrial dysfunction leads to deconjugation of quercetin glucuronides in inflammatory macrophages. PLoS One. 2013 Nov 19;8(11):e80843. doi: 10.1371/journal.pone.0080843.

62. Holloszy JO. Exercise-induced increase in muscle insulin sensitivity. J Appl Physiol (1985). 2005 Jul;99(1):338-43. doi: 10.1152/japplphysiol.00123.2005.

63. Cobley JN, Davison GW. Oxidative Eustress in Exercise Physiology (1st ed.). CRC Press. 2022. https://doi.org/10.1201/9781003051619

64. Mao Z, Hine C, Tian X, Van Meter M, Au M, Vaidya A, Seluanov A, Gorbunova V. SIRT6 promotes DNA repair under stress by activating PARP1. Science. 2011 Jun 17;332(6036):1443-6. doi: 10.1126/science.1202723.

65. Van Acker SA, van den Berg DJ, Tromp MN, Griffioen DH, van Bennekom WP, van der Vijgh WJ, Bast A. Structural aspects of antioxidant activity of flavonoids. Free Radic Biol Med. 1996;20(3):331-42. doi: 10.1016/0891-5849(95)02047-0.

66. Cadet J, Davies KJA. Oxidative DNA damage & repair: An introduction. Free Radic Biol Med. 2017 Jun;107:2-12. doi: 10.1016/j.freeradbiomed.2017.03.030.

67. Ristow M, Zarse K. How increased oxidative stress promotes longevity and metabolic health: The concept of mitochondrial hormesis (mitohormesis). Exp Gerontol. 2010 Jun;45(6):410-8. doi: 10.1016/j.exger.2010.03.014.

68. Gorbunova V, Seluanov A, Mao Z, Hine C. Changes in DNA repair during aging. Nucleic Acids Res. 2007;35(22):7466-74. doi: 10.1093/nar/gkm756.

69. Van Meter M, Simon M, Tombline G et al. JNK Phosphorylates SIRT6 to Stimulate DNA Double-Strand Break Repair in Response to Oxidative Stress by Recruiting PARP1 to DNA Breaks. Cell Rep. 2016 Sep 6;16(10):2641-2650. doi: 10.1016/j.celrep.2016.08.006.

70. Juan CG, Matchett KB, Davison GW. A systematic review and meta-analysis of the SIRT1 response to exercise. *Sci Rep*. 2023;13(1):14752. Available from: https://www.nature.com/articles/s41598-023-38843-x

71. Haigis MC, Sinclair DA. Mammalian sirtuins: biological insights and disease relevance. Annu Rev Pathol. 2010;5:253-95. doi: 10.1146/annurev.pathol.4.110807.092250.

72. White AT, Schenk S. NAD(+)/NADH and skeletal muscle mitochondrial adaptations to exercise. Am J Physiol Endocrinol Metab. 2012 Aug 1;303(3):E308-21. doi: 10.1152/ajpendo.00054.2012.

73. Ho CL, Kao NJ, Lin CI et al. Quercetin Increases Mitochondrial Biogenesis and Reduces Free Radicals in Neuronal SH-SY5Y Cells. Nutrients. 2022 Aug 12;14(16):3310. doi: 10.3390/nu14163310.

74. Xie R, Zhao W, Lowe S et al. Quercetin alleviates kainic acid-induced seizure by inhibiting the Nrf2-mediated ferroptosis pathway. Free Radic Biol Med. 2022 Oct;191:212-226. doi: 10.1016/j.freeradbiomed.2022.09.001.

75. Gurd BJ, Perry CG, Heigenhauser GJ, Spriet LL, Bonen A. High-intensity interval training increases SIRT1 activity in human skeletal muscle. Appl Physiol Nutr Metab. 2010 Jun;35(3):350-7. doi: 10.1139/H10-030.

76. Mostoslavsky R, Chua KF, Lombard DB, Pang WW, Fischer MR, Gellon L, et al. Genomic instability and aging-like phenotype in the absence of mammalian SIRT6. Cell. 2006;124(2):315-329. doi:10.1016/j.cell.2005.11.044

77. Michishita E, McCord RA, Berber E, Kioi M, Padilla-Nash H, Damian M, et al. SIRT6 is a histone H3 lysine 9 deacetylase that modulates telomeric chromatin. Nature. 2008;452(7186):492-496. doi:10.1038/nature06736

78. Toiber D, Erdel F, Bouazoune K, Silberman DM, Zhong L, Mulligan P, et al. SIRT6 recruits SNF2H to DNA break sites, preventing genomic instability through chromatin remodeling. Mol Cell. 2013;51(4):454-468. doi:10.1016/j.molcel.2013.06.018

79. Zhong L, D'Urso A, Toiber D et al. The histone deacetylase Sirt6 regulates glucose homeostasis via Hif1alpha. Cell. 2010 Jan 22;140(2):280-93. doi: 10.1016/j.cell.2009.12.041.

80. Pan H, Guan D, Liu X et al. SIRT6 safeguards human mesenchymal stem cells from oxidative stress by coactivating NRF2. Cell Res. 2016 Feb;26(2):190-205. doi: 10.1038/cr.2016.4.

81. Van Meter M, Mao Z, Gorbunova V, Seluanov A. Repairing split ends: SIRT6, mono-ADP ribosylation and DNA repair. Aging (Albany NY). 2011 Sep;3(9):829-35. doi: 10.18632/aging.100389.

82. Li Z, Luo A, Xie B. The Complex Network of ADP-Ribosylation and DNA Repair: Emerging Insights and Implications for Cancer Therapy. Int J Mol Sci. 2023 Oct 9;24(19):15028. doi: 10.3390/ijms241915028.

83. Geraets L, Moonen HJJ, Brauers K, Wouters EFM, Bast A, Hageman GJ. Dietary flavones and flavonoles are inhibitors of poly(ADP-ribose) polymerase-1 in pulmonary epithelial cells. J Nutr. 2007;137(10):2190-2195. doi:10.1093/jn/137.10.2190.

84. Kellenberger E, Kuhn I, Schuber F, Muller-Steffner H. Flavonoids as inhibitors of human CD38. Bioorg Med Chem Lett. 2011;21(12):3939-3942. doi:10.1016/j.bmcl.2011.04.119.

85. Boiteux S, Radicella JP. The human OGG1 gene: structure, functions, and its implication in the process of carcinogenesis. Arch Biochem Biophys. 2000;377(1):1-8. doi:10.1006/abbi.2000.1735.

86. Singh A, Venkannagari S, Oh KH, Zhang YQ, Rohde JM, Liu L, et al. Nrf2-dependent induction of OGG1 during oxidative stress is critical for repair of oxidized DNA lesions and cell survival. Free Radic Biol Med. 2013;56:16-25. doi:10.1016/j.freeradbiomed.2012.11.017.

87. Shang Y, Wang D, Wang X, Zhao Q, Li Y, Wang J, et al. Nrf2 signaling contributes to regulation of OGG1 in response to oxidative stress. Redox Biol. 2022;55:102404. doi:10.1016/j.redox.2022.102404.

88. Min K, Ebeler SE. Quercetin inhibits hydrogen peroxide-induced DNA damage and enhances DNA repair in Caco-2 cells. Food Chem Toxicol. 2009;47(11):2716-2722. doi:10.1016/j.fct.2009.07.025.

89. Jasin M, Rothstein R. Repair of strand breaks by homologous recombination. Cold Spring Harb Perspect Biol. 2013 Nov 1;5(11):a012740. doi: 10.1101/cshperspect.a012740.

90. Haince JF, Kozlov S, Dawson VL et al. Ataxia telangiectasia mutated (ATM) signaling network is modulated by a novel poly(ADP-ribose)-dependent pathway in the early response to DNA-damaging agents. J Biol Chem. 2007 Jun 1;282(22):16441-53. doi: 10.1074/jbc.M608406200.

91. Rajamohan SB, Pillai VB, Gupta M et al. SIRT1 promotes cell survival under stress by deacetylation-dependent deactivation of poly(ADP-ribose) polymerase 1. Mol Cell Biol. 2009 Aug;29(15):4116-29. doi: 10.1128/MCB.00121-09.

92. Hinz JM. Role of homologous recombination in DNA interstrand crosslink repair. Environ Mol Mutagen. 2010 Jul;51(6):582-603. doi: 10.1002/em.20577. PMID: 20658649.

93. Mao Z, Bozzella M, Seluanov A, Gorbunova V. Comparison of nonhomologous end joining and homologous recombination in human cells. DNA Repair (Amst). 2008 Oct 1;7(10):1765-71. doi: 10.1016/j.dnarep.2008.06.018.

94. Andrabi SA, Umanah GK, Chang C et al. Poly(ADP-ribose) polymerase-dependent energy depletion occurs through inhibition of glycolysis. Proc Natl Acad Sci U S A. 2014 Jul 15;111(28):10209-14. doi: 10.1073/pnas.1405158111.

95. Alano CC, Garnier P, Ying W, Higashi Y, Kauppinen TM, Swanson RA. NAD+ depletion is necessary and sufficient for poly(ADP-ribose) polymerase-1-mediated neuronal death. J Neurosci. 2010 Feb 24;30(8):2967-78. doi: 10.1523/JNEUROSCI.5552-09.2010.

96. Escande C, Nin V, Price NL et al. Flavonoid apigenin is an inhibitor of the NAD+ ase CD38: implications for cellular NAD+ metabolism, protein acetylation, and treatment of metabolic syndrome. Diabetes. 2013 Apr;62(4):1084-93. doi: 10.2337/db12-1139.

97. Xu Z, Zhang L, Zhang W et al. SIRT6 rescues the age related decline in base excision repair in a PARP1-dependent manner. Cell Cycle. 2015;14(2):269-76. doi: 10.4161/15384101.2014.980641.

98. Gudelj I, Lauc G, Pezer M. Immunoglobulin G glycosylation in aging and diseases. Cell Immunol. 2018;333:65-79. doi:10.1016/j.cellimm.2018.07.009.

99. Lauc G, Pezer M, Rudan I, Campbell H. Mechanisms of disease: The human N-glycome. Biochim Biophys Acta. 2013;1820(9):1493-1502. doi:10.1016/j.bbagen.2012.12.011.

100. Pucić M, Knežević A, Vidic J, Adamczyk B, Novokmet M, Polasek O, et al. High throughput isolation and glycosylation analysis of IgG-variability and heritability of the IgG glycome in three isolated human populations. Mol Cell Proteomics. 2011;10(10):M111.010090. doi:10.1074/mcp.M111.010090.

101. Antunes BM, Rossi FE, Cholewa JM, Lira FS. Regular exercise and immune system: what can we learn from the COVID-19 pandemic? Rev Bras Med Esporte. 2019;25(Suppl 1):60-67. doi:10.1590/1517-8692201925012019_0025.

102. Tijardović M, Marušić M, Brkanac SR, Grubić Z, Lauc G, Gornik O. Intense physical exercise induces anti-inflammatory changes in IgG N-glycosylation profile. Glycobiology. 2019;29(5):397-405. doi:10.1093/glycob/cwz013.

103. Cao Y, Song Z, Guo Z et al. Cytokines in the Immune Microenvironment Change the Glycosylation of IgG by Regulating Intracellular Glycosyltransferases. Front Immunol. 2022 Jan 24;12:724379. doi: 10.3389/fimmu.2021.724379.

104. Dewald JH, Colomb F, Bobowski-Gerard M et al. Role of Cytokine-Induced Glycosylation Changes in Regulating Cell Interactions and Cell Signaling in Inflammatory Diseases and Cancer. Cells. 2016 Nov 29;5(4):43. doi: 10.3390/cells5040043.

105. Wu ZH, Shi Y, Tibbetts RS, Miyamoto S. Molecular linkage between the kinase ATM and NF-kappaB signaling in response to genotoxic stimuli. Science. 2006 Feb 24;311(5764):1141-6. doi: 10.1126/science.1121513.

106. Rodier F, Coppé JP, Patil CK, Hoeijmakers WA, Muñoz DP, Raza SR, Freund A, Campeau E, Davalos AR, Campisi J. Persistent DNA damage signalling triggers senescence-associated inflammatory cytokine secretion. Nat Cell Biol. 2009 Aug;11(8):973-9. doi: 10.1038/ncb1909.

107. Hinz M, Stilmann M, Arslan SÇ, Khanna KK, Dittmar G, Scheidereit C. A cytoplasmic ATM-TRAF6-cIAP1 module links nuclear DNA damage signaling to ubiquitin-mediated NF-κB activation. Mol Cell. 2010 Oct 8;40(1):63-74. doi: 10.1016/j.molcel.2010.09.008.

108. Khoder-Agha F, Kietzmann T. The glyco-redox interplay: Principles and consequences on the role of reactive oxygen species during protein glycosylation. Redox Biol. 2021;43:101962. https://doi.org/10.1016/j.redox.2021.101888.

109. Alborzinia H, Ignashkova TI, Dejure FR, Gendarme M, Theobald J, Wölfl S, Lindemann RK, Reiling JH. Golgi stress mediates redox imbalance and ferroptosis in human cells. Commun Biol. 2018 Nov 28;1:210. doi: 10.1038/s42003-018-0212-6.

110. Kellokumpu S. Golgi pH, Ion and Redox Homeostasis: How Much Do They Really Matter? Front Cell Dev Biol. 2019 Jun 11;7:93. doi: 10.3389/fcell.2019.00093.

111. Hossler P, Khattak SF, Li ZJ. Optimal and consistent protein glycosylation in mammalian cell culture. Glycobiology. 2009 Sep;19(9):936-49. doi: 10.1093/glycob/cwp079.

112. Varki A et al. (eds). *Essentials of Glycobiology.* 4th ed. Cold Spring Harbor Laboratory Press; 2022.

113. Maverakis E, Kim K, Shimoda M et al. Glycans in the immune system and the altered glycan theory of autoimmunity: A critical review. J Autoimmun. 2015 Feb;57:1-13. doi: 10.1016/j.jaut.2014.12.002.

114. Šimunić-Briški N, Dukarić V, Očić M et al. Regular moderate physical exercise decreases Glycan Age index of biological age and reduces inflammatory potential of Immunoglobulin G. Glycoconj J. 2024 Feb;41(1):67-76. doi: 10.1007/s10719-023-10144-5.

115. Pribić T, Das JK, Đerek L et al. A 2-year calorie restriction intervention may reduce glycomic biological age biomarkers - a pilot study. NPJ Aging. 2025 Aug 1;11(1):71. doi: 10.1038/s41514-025-00254-9.